

An adaptive step size controller for iterative implicit methods[☆]

Lukas Einkemmer^{a,*}

^a*Department of Mathematics, University of Innsbruck, Austria*

Abstract

The automatic selection of an appropriate time step size has been considered extensively in the literature. However, most of the strategies developed operate under the assumption that the computational cost (per time step) is independent of the step size. This assumption is reasonable for non-stiff ordinary differential equations and for partial differential equations where the linear systems of equations resulting from an implicit integrator are solved by direct methods. It is, however, usually not satisfied if iterative (for example, Krylov) methods are used.

In this paper, we propose a step size selection strategy that adaptively reduces the computational cost (per unit time step) as the simulation progresses, constraint by the tolerance specified. We show that the proposed approach yields significant improvements in performance for a range of problems (diffusion-advection equation, Burgers' equation with a reaction term, porous media equation, viscous Burgers' equation, Allen–Cahn equation, and the two-dimensional Brusselator system). While traditional step size controllers have emphasized a smooth sequence of time step sizes, we emphasize the exploration of different step sizes which necessitates relatively rapid changes in the step size.

Keywords: adaptive step size selection; implicit time integration; iterative methods

1. Introduction

Numerically solving time dependent differential equations is an important task in many fields of science and engineering. Crucial to that process is an efficient time integrator. Since the early advent of computers such methods have been used to first solve ODEs (ordinary differential equation) and then PDEs (partial differential equations).

Numerical simulations can be run with a constant time step size. However, modern software packages usually automatically select an appropriate step size given a desired tolerance (which is specified by the user). To accomplish this so-called (automatic) step size controllers are used in conjunction with an error estimator. Such an approach provides a range of advantages. First, it frees the user from selecting an appropriate step size and, ideally, from verifying the accuracy of the simulation (by numerical convergence studies or similar means). Second, a good step size controller is not only able to provide an estimate of the error made, but also to detect the onset of numerical instabilities and to reduce the step size to prevent them. This is of particular importance for explicit methods which, for example, can not operate with step sizes above the Courant–Friedrichs–Lewy (CFL) limit and for implicit methods that are not A-stable. Last, but certainly not least, step size controllers can increase the computational efficiency by allowing the software to adaptively increase and decrease the step size during the course of the simulation. This is usually done in response to an error estimate, where errors significantly below the specified tolerance indicate the possibility to increase the time step.

Step size controllers require an error estimate. Fortunately, estimating the error can often be accomplished with only a minor increase in the computational cost. One approach commonly used are so-called embedded

*Corresponding author

Email address: lukas.einkemmer@uibk.ac.at (Lukas Einkemmer)

Runge–Kutta methods. These schemes consist of a pair of Runge–Kutta methods with different order that share most or even all internal stages (see, for example, [12, Chap. II.4] or [4, 5, 20]). For multistep methods a comparison with extrapolated values is often used (see, for example, [14]). Alternatively, Richardson extrapolation can be used to obtain an error estimate, but is usually more demanding from a computational point of view.

Almost all step size controllers are predicated on the assumption that the largest possible step size should be selected. Thus, the step size is chosen such that the error committed exactly matches the tolerance specified by the user. This is a reasonable assumption for explicit Runge–Kutta methods, where the computational cost is independent of the step size. Now, let us assume that our error estimator provides an estimate e^k for the k th step (note that in accordance with much of the PDE literature we use superscripts to denote the time indices). The local error of a numerical method with order p is modeled as $e^k = D(\tau^k)^{p+1}$, where τ denotes the time step size and D is a constant (which for the purpose of simplicity is assumed to be independent of k ; in most situations this is a reasonable assumption as the error constant only varies slowly on $\mathcal{O}(\tau)$ timescales). Then, to determine the optimal step size we set

$$\text{tol} = e^{k+1} = D(\tau^{k+1})^{p+1},$$

where tol is the user specified tolerance. This is not a particularly useful constraint to determine τ^{k+1} as D is unknown. Thus, we consider

$$\frac{e^{k+1}}{e^k} = \left(\frac{\tau^{k+1}}{\tau^k} \right)^{p+1}$$

which can be solved for τ^{k+1}

$$\tau^{k+1} = \tau^k \left(\frac{\text{tol}}{e^k} \right)^{1/p}. \quad (1)$$

Equation (1) allows us to estimate the optimal time step τ^{k+1} based on the previous error estimate e^k and the previous time step size τ^k . This then results in a sequence of times t^k at which a numerical approximation is obtained. In practice this is a dangerous approach as even very small errors in the error estimate can result in a time step sizes that exceeds the prescribed tolerance (leading to step size rejection). Thus, usually a safety factor is incorporated. For more details we refer the reader to [12, Chap. II.4] and [19].

This simple formula can be interpreted as a P controller. The mathematical analysis is in fact based on this observation (see, for example, [9, 8, 21, 22]). Consequently, PI controllers have been introduced [9], which for some integrators and problems show an increase in performance. Certainly, these PI controllers increase the smoothness of the step size sequence (i.e. the change in step size behaves less erratic). These ideas have been enhanced in a variety of directions. The importance of changing strategies when operating close to the stability limit for explicit methods has also been recognized [13].

Although some work has been conducted in estimating global errors (see, for example, [19]), the local step size controllers described above, with some modifications to avoid excessively large step sizes, still form the backbone of most time integration packages. For example, the RADAU5 code [11, Chap. IV.8] employs a variant of the PI controller, while the multistep based CVODE code [14] and [6] uses a variant of the P controller. As a result, the described step size controllers have been extensively tested and used in a range of applications, both for ordinary as well as for partial differential equations.

The desire for solving partial differential equations with ever increasing grid sizes and more accurate physical models, however, calls into question the validity of the assumptions made. In both the RADAU5 and CVODE code mentioned above implicit numerical methods are employed to solve the stiff ODEs resulting from the space discretization of the PDE under consideration. These implicit methods require the solution of a linear system of equations which is now routinely done by iterative numerical methods (such as the conjugate gradient method or GMRES). However, the number of iterations required is quite sensitive to the linear system solved. In particular, smaller time step sizes reduce the magnitude of the largest eigenvalue of the matrix, which in turn reduces the number of iterations required per time step. This means that reducing the time step size below what is dictated by the specified tolerance, e.g. according to equation (1), can actually result in an increase in performance.

Many implementations do not exploit this fact. However, the issue at hand has been recognized in [15] and [24]. Both of these approaches limit the size of the Krylov subspace. In [15] both lower and upper bounds are specified. If the Krylov dimension falls within those bounds, the time step size is chosen according to the step size controller. If this is not the case, the step size is adjusted. In [24] a multiple Arnoldi process is used. In that context the increase of the Krylov dimension in the higher stages is limited by a fixed value. The downside of this approach is that it is usually not known a priori how the bounds should be chosen; the corresponding value is most likely highly problem dependent. It should also be noted that in the context of ODEs the importance of considering variations in cost (as a function of the time step size) has been recognized in [10]. There are analytically derived estimates of the cost and, in line with the control theoretic approach to step size selection, smooth step size sequences have been emphasized. In contrast, in this work we emphasize dynamically obtained estimates of the cost (which is particularly useful for nonlinear PDEs, where obtaining good a priori estimates is often extremely difficult) and exploration of the space of admissible step sizes (which results in rather frequent and often erratic step size changes). Furthermore, in the context of approximating matrix exponentials by polynomial interpolation at Leja points, a procedure to determine the optimal step size based on a backward error analysis has been proposed [3]. This approach can be very effective but requires certain information on the spectrum of the matrix under consideration. This information is not easily obtained in a matrix free implementation and, for nonlinear PDEs, can change from one time step to the next. In contrast, the step size controller proposed in this work requires no a priori information and is thus designed to naturally work for matrix free implementations.

In addition to the considerations above, it has been observed in many applications that a reversed C shape can be observed on a precision-work diagram for the traditional step size controllers. That is, specifying a more stringent tolerance initially results in an increase of performance (i.e. smaller run times). The problem with that approach is that the user of the software is once again tasked with finding the best step size (or rather decreasing the tolerance until the run time is minimized as well). Thus, effectively counteracting one of the primary advantages of automatic step size control.

Such behavior can be observed across a range of test problems [16, 17, 15] as well as for problems that stem from more realistic physical models [7, 2, 18]. As the before mentioned work shows, this behavior is not limited to one class of numerical method but can be observed for implicit Runge-Kutta methods, BDF methods, implicit-explicit (IMEX) methods, and exponential integrators.

In this paper we propose an approach for adaptive step size control that does not optimize for the largest time step size but rather tries to minimize computational cost. Since it is difficult to analytically determine the optimal step size, an optimization procedure is used in parallel with the time stepper. The basic idea of this algorithm is described in section 2. There numerical results for a linear diffusion-advection equation are also shown. In section 3 the efficiency of our algorithm applied to four nonlinear problems is investigated. Finally, we conclude in section 5.

2. Basic algorithm

2.1. Setting

For the remainder of this section we consider the linear diffusion-advection equation

$$\partial_t u(t, x) = \partial_{xx} u(t, x) + \eta \partial_x u(t, x) \quad (2)$$

with periodic boundary conditions on $[0, 1]$. The dimensionless Péclet number η determines the relative strength of advection compared to diffusion. As initial value we prescribe the following Gaussian

$$u(0, x) = e^{-(x-1/2)^2/(2\sigma_0^2)}.$$

In this setting the analytic solution is known exactly (strictly speaking this is only true if the problem is posed on the entire real line; however, for times where the spread of the Gaussian is smaller than the computational domain, a similar dynamics can be observed for periodic boundary conditions). The Gaussian is translated in space and the bump spreads out (assuming that the solution is sufficiently small at the boundary). The

spread of the standard deviation σ at time t is given by $\sigma(t) = \sqrt{\sigma_0^2 + 2t}$. In particular, this implies that if a small σ_0 is chosen the time step size is initially dictated by accuracy constraints (even for small Péclet numbers). However, later in the evolution implicit time integrators can take relatively large time steps without incurring a significant error. In the numerical simulations conducted we will choose a final time $t = 0.2$. Thus, the present test problem probes both of these regimes.

Note that in the numerical simulations we will present, advection dominated (i.e. large η) processes are considered as well. In this regime, an explicit numerical methods could also be used. However, it is our view that a general purpose implicit integrator/step size controller should also be able to handle such problems. We will see, however, that this is a challenging problem for the traditional step size controller.

In all our implementations we use the standard centered difference scheme to discretize the diffusive part and a simple upwind scheme for the advection. Concerning the time discretization, implicit Runge–Kutta methods will be employed. This is done in order to avoid some of the tedious details encountered when dealing with variable step size multistep methods (for example, limitations on how rapidly the time step size is allowed to change).

Many implicit Runge–Kutta method have been considered in the literature. Perhaps, the most well known are the Crank–Nicolson method and the classes of Gauss and Radau methods. The latter forms the basis for the widely used RADAU5 time integrator. However, the issue with higher order collocation methods is that a straightforward implementation yields large matrices to invert. This further worsens the problem that we try to overcome in this paper (see below) which incidentally would lead to overly optimistic results. In addition, almost all of the publicly available integrator packages either do not directly support sparse Krylov solvers (such as RADAU5), make it very difficult to change the time stepping strategy or to specify a fixed order or fixed time step size (such as CVODE). Thus, in the following we will use the Crank–Nicolson scheme along with a two stage third order SDIRK (singly diagonally implicit) scheme, henceforth called SDIRK23, and a five stage fourth order SDIRK scheme, henceforth called SDIRK54. All of these methods require us to (only) solve an $n \times n$ linear system, where n is the number of grid points and thus give a better indication of the actual performance attainable. The same can be accomplished for an implementation of Radau methods (see, for example, [11, Chap. IV.8]) but in this case the details of the implementation are much more involved. This is a further reason to stick with the, relatively simple, Crank–Nicolson, SDIRK23, and SDIRK54 method.

Now, let us describe the numerical time integrators used in this paper in more detail. After an appropriate discretization in space we have to integrate the following system of ODEs (ordinary differential equations)

$$y'(t) = f(t, y(t))$$

in time. For linear autonomous problems this ODE could be significantly simplified. However, since we will encounter nonlinear problems in section 3 we will consider the more general formulation here. In this setting the Crank–Nicolson scheme is given by

$$y^1 = y^0 + \frac{\tau}{2} (f(0, y^0) + f(\tau, y^1)),$$

where the time step size of τ is conducted to obtain y^1 from y^0 . The third order SDIRK23 scheme is given by (see, for example, [1])

$$\begin{aligned} k^1 &= f(\gamma\tau, y^0 + \tau\gamma k^1) \\ k^2 &= f((1-\gamma)\tau, y^0 + (1-2\gamma)\tau k^1 + \gamma\tau k^2) \\ y^1 &= y^0 + \frac{\tau}{2} (k^1 + k^2), \end{aligned}$$

where $\gamma = \frac{3+\sqrt{3}}{6}$. For a linear problem (i.e. $f(t, y(t)) = Ay(t)$ for $A \in \mathbb{R}^{n \times n}$) this yields

$$\begin{aligned}(I - \tau\gamma A)k^1 &= Ay^0 \\ (I - \tau\gamma A)k^2 &= Ay^0 + (1 - 2\gamma)\tau Ak^1 \\ y^1 &= y^0 + \frac{\tau}{2}(k^1 + k^2).\end{aligned}$$

Thus, we only have to solve two $n \times n$ linear systems. In the nonlinear case this is still true but the linear solve is now conducted as the inner loop in Newton's method. The SDIRK54 scheme is given by [11, p. 107]

$$\begin{aligned}k^1 &= \tau f\left(\frac{1}{4}\tau, y^0 + \frac{1}{4}k^1\right) \\ k^2 &= \tau f\left(\frac{3}{4}\tau, y^0 + \frac{1}{2}k^1 + \frac{1}{4}k^2\right) \\ k^3 &= \tau f\left(\frac{11}{20}\tau, y^0 + \frac{17}{50}k^1 - \frac{1}{25}k^2 + \frac{1}{4}k^3\right) \\ k^4 &= \tau f\left(\frac{1}{2}\tau, y^0 + \frac{371}{1360}k^1 - \frac{137}{2720}k^2 + \frac{15}{544}k^3 + \frac{1}{4}k^4\right) \\ k^5 &= \tau f\left(\tau, y^0 + \frac{25}{24}k^1 - \frac{49}{48}k^2 + \frac{125}{16}k^3 - \frac{85}{12}k^4 + \frac{1}{4}k^5\right) \\ y^1 &= y^0 + \frac{25}{24}k^1 - \frac{49}{48}k^2 + \frac{125}{16}k^3 - \frac{85}{12}k^4 + \frac{1}{4}k^5.\end{aligned}$$

This SDIRK54 method is L-stable. The Crank–Nicolson method and the SDIRK23 method are A-stable but not L-stable. Even though we use A-stable implicit methods here it is instructive to consider the stability constraints that the explicit Euler method would encounter. In this case we have

$$\tau < \min\left(\frac{1}{2n^2}, \frac{1}{|\eta|n}\right),$$

where n , as before, denote the number of grid points. Usually, this is dominated by the stability constraint from the diffusion (the first term in the formula) but we will also consider examples where the Péclet number is large enough such that these two stability constraints are comparable.

In all our examples we will use the GMRES (generalized minimal residual) method to solve the resulting linear system (note that for $\eta \neq 0$ the matrix A is not symmetric). This iterative Krylov subspace method terminates when the residual is below one-tenth of the tolerance prescribed for the numerical method. It should be emphasized, however, that the step size controller proposed in the next section is completely independent of the iterative method used. The choice of Krylov methods is due to their ubiquity in applications. Nonetheless, relaxation methods or methods based on (direct) polynomial interpolation could be used just as easily (as all the relevant data are obtained at run time).

2.2. Step size controller

As has been outlined in the introduction, traditional step size controller always take the largest step possible given the accuracy constraints. In our case, we will adaptively change the step size depending on the cost of the previous time step. This allows us to explore a range of step sizes and search for the most cost effective one (which might be significantly smaller than the one selected by a traditional step size controller). In the following we will interpret this as a one-dimensional gradient descent optimization algorithm.

Our goal is to optimize the computational cost per unit time step, i.e.

$$c^k = \frac{M(i^k)}{\tau^k},$$

where i^k is the number of Krylov iterations conducted in the k th time step (i.e. the sum of the Krylov dimensions over all stages of the method) and τ^k is the size of the step. The function $M: \mathbb{N} \rightarrow \mathbb{R}_{\geq 0}$ models the computational cost as a function of the number of iterations. This is not a trivial task and the function M , in general, depend on the computer system used. For example, on large scale supercomputers the latency introduced by the dot products can actually be the limiting factor with respect to performance. The situation

is further complicated by the fact that GMRES has to be used with a restart procedure (in our simulation we will restart every 20th iterations). In the present work we will assume that the computational cost is directly proportional to the number of iterations; i.e. $M(i^k) = i^k$. This assumption is valid if the cost of the dot products is small compared to the cost of evaluating the right-hand side of the PDE. However, we duly note that the controller presented in the following can be used just as well with a different cost model M and that there are certainly situations where this would be indicated.

Since the number of Krylov iterations is determined adaptively, the cost is only available at the end of the time step. Our goal is to dynamically adjust the step size (i.e. to change τ^k) such that

$$c^k \rightarrow \min.$$

As is usually done in the analysis of step size controllers, we work with the logarithm of the step size $T^k = \log \tau^k$ and the logarithm of the computational cost $C^k(T^k) = \log c^k(\tau^k)$. Employing a one-dimensional gradient descent algorithm we have (assuming that the cost per unit step C^k is only a function of the time step size T^k)

$$T^{k+1} = T^k - \gamma \nabla C^k(T^k)$$

Now, since we have only discrete values at our disposal we approximate the gradient by a difference quotient

$$\nabla C^k(T^k) \approx \frac{C^k(T^k) - C^k(T^{k-1})}{T^k - T^{k-1}}.$$

By doing so we effectively rule out taking a constant time step size (i.e. $T^k = T^{k-1}$). This is necessary in order to obtain the necessary information that guide our adaptive step size selection. In the literature it is often argued that a smooth step size selection is desirable in order to increase the accuracy of the error estimator. However, in our case we will only use the error estimator as a worst case bound. Most of the time, the step size will be chosen well below that limit. This implies that step size rejection happens infrequently (if at all) even if the time step size varies considerably from one step to the next.

Unfortunately, making this approximation is not yet sufficient as, strictly speaking, we have to make a distinction between the cost functions C^{k-1} and C^k . Note that $C^{k-1}(T)$ gives the cost of making a step with size T starting from the beginning of the previous time step, i.e. starting from t^{k-1} . This value is, in general, different from $C^k(T)$ (the cost of making a step with the same size but starting at t^k). During the time integration only $C^{k-1}(T^{k-1})$ but not $C^k(T^{k-1})$ is sampled. Thus, we write

$$\frac{C^k(T^k) - C^k(T^{k-1})}{T^k - T^{k-1}} = \frac{C^k(T^k) - C^{k-1}(T^{k-1})}{T^k - T^{k-1}} + \frac{C^{k-1}(T^{k-1}) - C^k(T^{k-1})}{T^k - T^{k-1}}.$$

Further assuming that C^k changes slowly as a function of k we obtain

$$\nabla C^k(T^k) \approx \frac{C^k(T^k) - C^{k-1}(T^{k-1})}{T^k - T^{k-1}}.$$

This then gives us

$$T^{k+1} = T^k - \gamma \frac{C^k(T^k) - C^{k-1}(T^{k-1})}{T^k - T^{k-1}}$$

In principle γ is a free parameter (which can depend on both c and τ). Taking the exponential on both sides gives

$$\tau^{k+1} = \tau^k \exp(-\gamma \Delta) \tag{3}$$

with

$$\Delta = \frac{\log c^k - \log c^{k-1}}{\log \tau^k - \log \tau^{k-1}}.$$

The simplest choice is taking $\gamma = \text{const}$ which, however, has two major drawbacks. First, if the cost varies rapidly for a relatively small change in τ we obtain extremely large time step changes. Second, if the cost

varies slowly we might only change the time step very slowly which means we can not explore the available parameter space efficiently. In fact, as we will see later, this ability to change the time step size even if Δ is small will be a crucial ingredient of our step size controller. Therefore, we propose to use the following method to determine the new time step size $\bar{\tau}^{k+1}$ from the old time step size τ^k

$$s = \exp(-\alpha \tanh(\beta \Delta))$$

$$\bar{\tau}^{k+1} = \tau^k \begin{cases} \lambda & 1 \leq s < \lambda \\ \delta & \delta \leq s < 1 \\ s & \text{otherwise} \end{cases} \quad (4)$$

which can be realized by choosing $\gamma(\Delta)$ in equation (3). This ensures that the time step size is changed by at least $\lambda\tau^k$ or $\delta\tau^k$ and limits the maximum step size change to $\exp(\pm\alpha)\tau^k$. The understanding here is that the parameters α, β, δ and λ are positive and that $\lambda > 1$ and $\delta < 1$ are sufficiently separated from 1 in order to always cause a non-trivial change in step size. The new time step size $\bar{\tau}^{k+1}$ is used only if it is smaller or equal to the time step size determined from the traditional controller. This is necessary as there is no guarantee that the step size computed from equation (4) satisfies the accuracy requirement specified by the user. That is, in all simulations we employ

$$\tau^{k+1} = \min\left(\bar{\tau}^{k+1}, \tau^k \left(\frac{\text{tol}}{e^k}\right)^{1/p}\right). \quad (5)$$

Limiting ourselves to a functional representation with four free parameters implies that we obtain a manageable optimizing problem for these parameters. The goal function is set by considering the average performance for $(n, \eta) \in \mathcal{N} = \{(100, 10), (300, 100), (500, 0), (500, 1000)\}$ and $\epsilon \in \mathcal{E} = \{10^{-2}, 10^{-3}, 10^{-4}, 10^{-5}, 10^{-7}\}$, where ϵ is the tolerance specified for the numerical method. We integrate until final time $t = 0.2$ and use the SDIRK54 method with $\sigma_0 = 1.4 \cdot 10^{-3}$ for the initial value. We consider the two fitness functions $f_1(\Gamma)$ and $f_2(\Gamma)$, depending on the parameter $\Gamma = (\alpha, \beta, \lambda, \delta)$, given by

$$f_1(\Gamma) = \sum_{(n, \eta) \in \mathcal{N}} \sum_{\epsilon \in \mathcal{E}} R_{n\eta\epsilon}(\Gamma)$$

and

$$f_2(\Gamma) = \sum_{(n, \eta) \in \mathcal{N}} \sum_{\epsilon \in \mathcal{E}} Q_{\Pi}(R_{n\eta\epsilon}(\Gamma), T_{n\eta\epsilon}),$$

where $R_{n\eta\epsilon}(\Gamma)$ is the run time of our step size controller with parameter Γ for the linear diffusion-advection problem specified by (n, η, ϵ) , $T_{n\eta\epsilon}$ is the run time required by the traditional step size controller for the same problem, and

$$Q_{\Pi}(x, y) = \frac{x}{y} \cdot \begin{cases} 1 & x/y \leq 1 \\ \Pi & \text{otherwise} \end{cases}.$$

The constant parameter Π penalizes cases where our approach performs worse than the traditional step size controller. This penalty parameter is used to trade off increased gain in performance (in, hopefully, the majority of configurations) with how much reduction in performance we are willing to tolerate (for, hopefully, a small number of configurations).

In the following we will consider two step size controllers based on $f_1(\Gamma)$ and $f_2(\Gamma)$ with penalty parameter $\Pi = 10$. A numerical optimization using differential evolution is performed. For the former case this results in the set of parameters

$$\alpha = 0.65241444, \quad \beta = 0.26862269, \quad \lambda = 1.37412002, \quad \delta = 0.64446017.$$

while the latter case gives

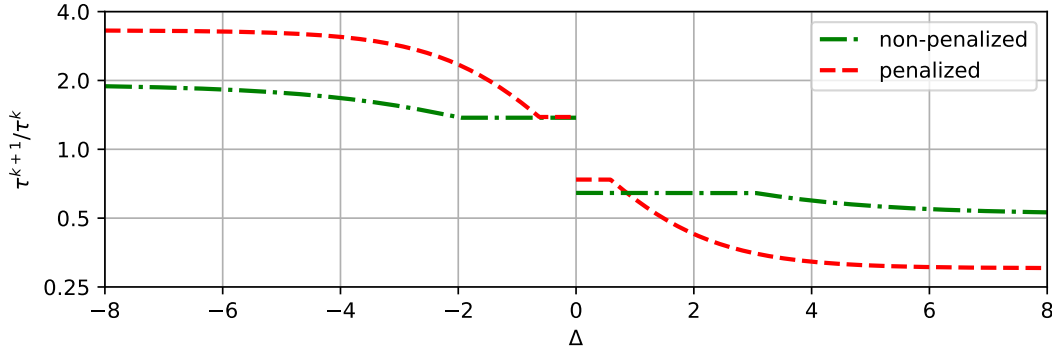


Figure 1: The ratio of the new step size to the old step size (i.e. τ^{k+1}/τ^k) is shown as a function of Δ for both the non-penalized (green dash-dotted line) and the penalized step size controller (red dashed line).

$$\alpha = 1.19735982, \quad \beta = 0.44611854, \quad \lambda = 1.38440318, \quad \delta = 0.73715227,$$

We will refer to these two sets of parameters (and to the corresponding step size controller) as the non-penalized and the penalized controller, respectively. The corresponding curves given by (4) are shown in Figure 1. The difference between these two can be understood as follows. For the penalized integrator it is often favorable to relatively rapidly increase the time step size in order to quickly reach the upper limit dictated by the accuracy requirement. If this regime is reached, the penalized step size controller effectively acts like the traditional controller (with the difference that it can still decrease the step size repeatedly in order to check if a smaller step size reduces the computational cost). For the non-penalized controller the goal is to more closely follow the gradient to find the (locally) most efficient time step size. This means that it has less variation in the time step size.

It can also be observed from Figure 1 that the minimal change in the step size is at least 30%. This results in the discontinuity seen in the plot at $\Delta = 0$ and supports our assertion that the step size should be varied rapidly in order to collect the data necessary for our algorithm.

In this work we will compare the step size controller proposed in this section with the traditional P controller. We choose the P controller (as opposed to a PI controller or any of the other extensions that have been developed) for two primary reasons. First, the P controller is still widely used in software packages such as CVODE [14] and the advantage more elaborate schemes can provide depends on the numerical method and a range of other factors. For example, in [23] it is shown that the PI controller fails to give good results for certain multistep methods. Second, the P controller is a simpler algorithm that only includes a single parameter (the safety factor) and most of the results achieved carry over easily to more elaborate methods.

2.3. Numerical results

We will use exactly the setup described in section 2.1. For the initial value we choose $\sigma_0 = 1.4 \cdot 10^{-3}$ and integrate until time $t = 0.2$. In Figure 2 the work-precision diagram for the Crank–Nicolson method is shown for the linear diffusion-advection equation. The cost (on the x -axis) is represented as the number of Krylov iterations required to advance the numerical solution by the same amount as the maximal step size allowed by the classic CFL condition (i.e. the number of Krylov iterations is normalized to the cost of an explicit Euler method that is operated with unit CFL number). The tolerance specified by the user is shown on the y -axis. The blue line for the traditional step size controller (a P controller with safety factor 0.9) shows the characteristic reversed C shaped curve mentioned in the introduction. Ideally, we would expect from a step size controller a monotonous increase in the cost as the tolerance is increased. We can see from 2 that the step size controller proposed in section 2.2 (the dashed red and dash-dotted blue line in the figure) matches this pattern very well (for a range of grids and different Péclet numbers). Instead of the reversed C shaped curve we now have, in almost all cases, a monotonously increase of cost as a function of tolerance.

What is perhaps even more important is the significant decrease in computational cost that is obtained by straightening out the reversed C curve. The actual increase in computational performance varies with the specific configuration but can yield a speedup of up to a factor of four. We also see that the non-penalized variants gives generally better results.

Let us discuss this results in more detail. In Figure 3 the step size for both the traditional controller (dashed lines) and the proposed controller (the non-penalized variant) are shown for four different tolerances. As has been discussed in the previous section, the maximal allowable time step (due to accuracy constraints) increases with time. This is in fact, what we observe for the traditional step size controller. In the beginning of the simulation this curve is very closely followed by our step size controller as well. This is to be expected as in this case the integrator operates very close to the accuracy limit. Later on, however, our step size controller only increases the time step size if this results in reduced computational cost (independent of accuracy constraints). This results in significantly smaller time steps which in turn results in a significant reduction in computational cost. This has the additional benefit that the numerical solution is more accurate than the tolerance requested indicates (see Figure 4 and the following discussion). Figure 3 also shows that our algorithm dictates a rapid change of step sizes. This is in stark contrast to the work on control theoretic step size selection, where it was often argued that a good control system should provide a smooth response [9, 22]. In our scheme, however, this rapid change is an important feature in order to collect the necessary information to guide step size selection (as has been discussed in the previous section).

The results in Figure 2 do not provide information on the actual global error that is achieved in the simulation. The behavior of the global error can, of course, be significantly different from the local error. The behavior of the corresponding error propagation, for example, depends on the problem under consideration. However, since the proposed step size controller is only able to decrease the time step size compared to the traditional approach, the local error per unit time step committed by the time integration scheme is also reduced. This then implies that the global error of the proposed controller is similar or smaller than the global error for the traditional approach. To illustrate this we plot, in Figure 4, the global error at the final time as a function of the Krylov iterations. If we compare these results to Figure 2 we can see that the advantage of the proposed step size controllers is even more pronounced according to that metric.

Similar simulations have been conducted for the SDIRK23 and SDIRK54 schemes. These are shown in Figures 5 and 6, respectively. The results are similar to the one discussed in detail for the Crank–Nicolson method. Although we also see that for (probably unrealistically) high Péclet numbers the traditional step size controller can slightly outperform the proposed method. Nevertheless, overall the results reinforce the significant advantage in performance the proposed method provides.

3. Nonlinear problems

While the linear example in the previous section illustrates very well the issues with standard step size controllers, ultimately we are not primarily interested in solving linear diffusion-advection equations. In addition, an integrator optimized for a rather restricted class of linear problems is not of much utility in practice. Thus, in this section we will consider a number of nonlinear problems to demonstrate that the proposed step size controller also works well in this regime.

3.1. Burgers' equation with a reaction term

As our first example we consider

$$\partial_t u(t, x) = \eta u(t, x) \partial_x u(t, x) + g(u(t, x)), \quad (6)$$

where we have chosen $g(u) = 10(u - 2)\sqrt{|u - 1|}$. As usual periodic boundary conditions on $[0, 1]$ are used and the following initial value is imposed

$$u(0, x) = 2 + \epsilon_1 \sin(\omega_1 x) + \epsilon_2 \sin(\omega_2 x + \varphi)$$

with $\epsilon_1 = \epsilon_2 = 10^{-2}$, $\omega_1 = 2\pi$, $\omega_2 = 8\pi$, and $\varphi = 0.3$. The nonlinear reaction satisfies $g(u) < 0$ for $u < 2$ and $g(u) > 0$ for $u > 0$. Thus, the perturbation introduced in the initial value results in parts of the solution

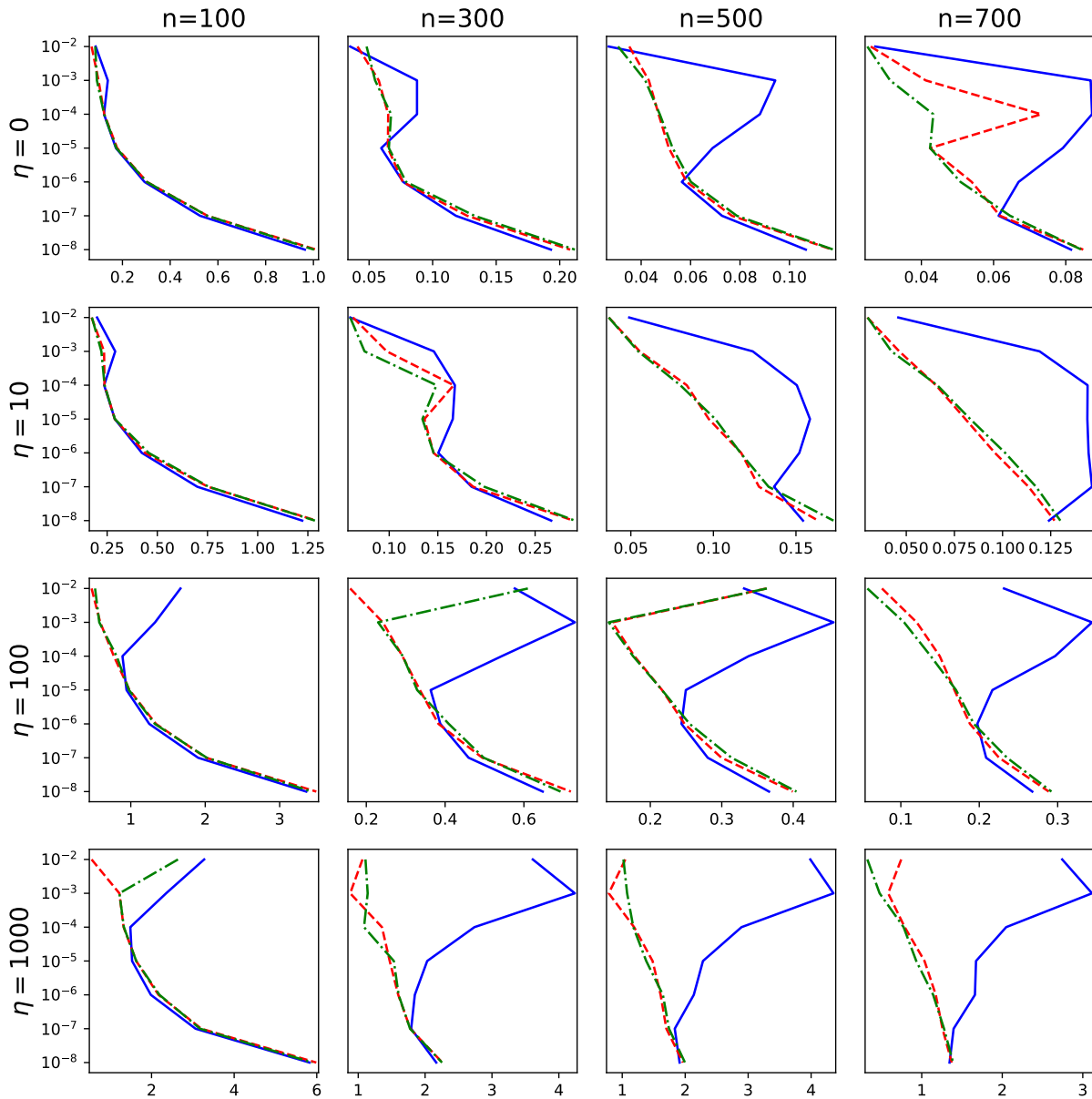


Figure 2: The number of normalized Krylov iterations employed by the Crank–Nicolson scheme (i.e. computational cost; on the x -axis) for a given tolerance (on the y -axis) is shown for equation (2) (linear diffusion-advection equation). The proposed step size controllers are shown as dashed red lines (penalized variant) and dash-dotted green lines (non-penalized variant), while the traditional step size controller is shown in solid blue. The grid size (n is the number of grid points) and the Péclet number η are varied.

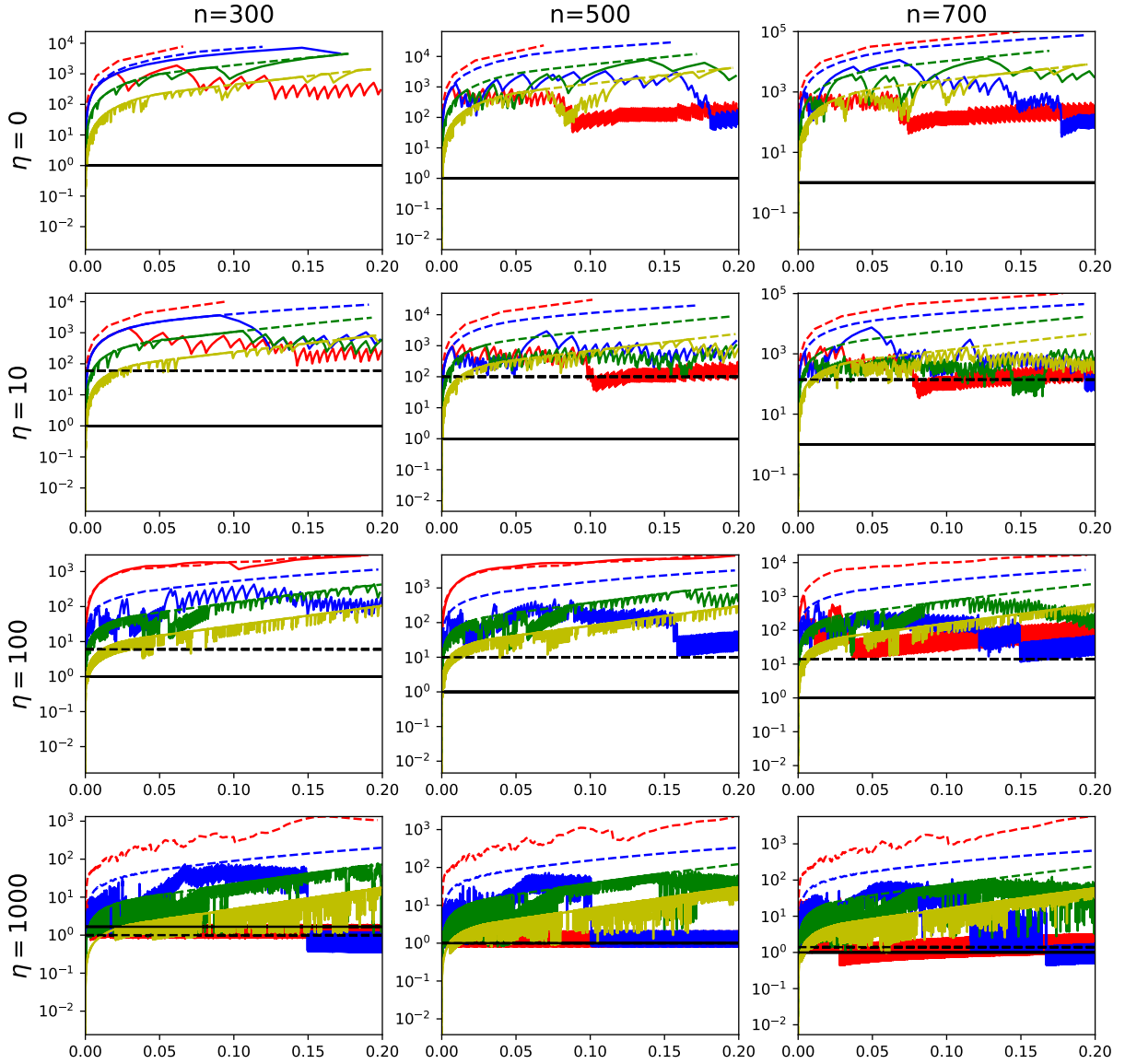


Figure 3: The CFL number (i.e. size of the time step divided by the maximal stable time step for the Euler method) taken by the Crank–Nicolson scheme is shown as a function of time (for the linear diffusion–advection equation (2)). The solid lines correspond to the proposed step size controller (the non-penalized variant), while dashed lines correspond to the classic step size controller. In both cases results for the tolerance set to 10^{-2} (red), 10^{-4} (blue), 10^{-6} (green), and 10^{-8} (yellow) are shown. The black line shows the CFL condition induced by the diffusion and the dashed black line shows the CFL condition induced by the advection. The grid size (n is the number of grid points) and the Péclet number η are varied.

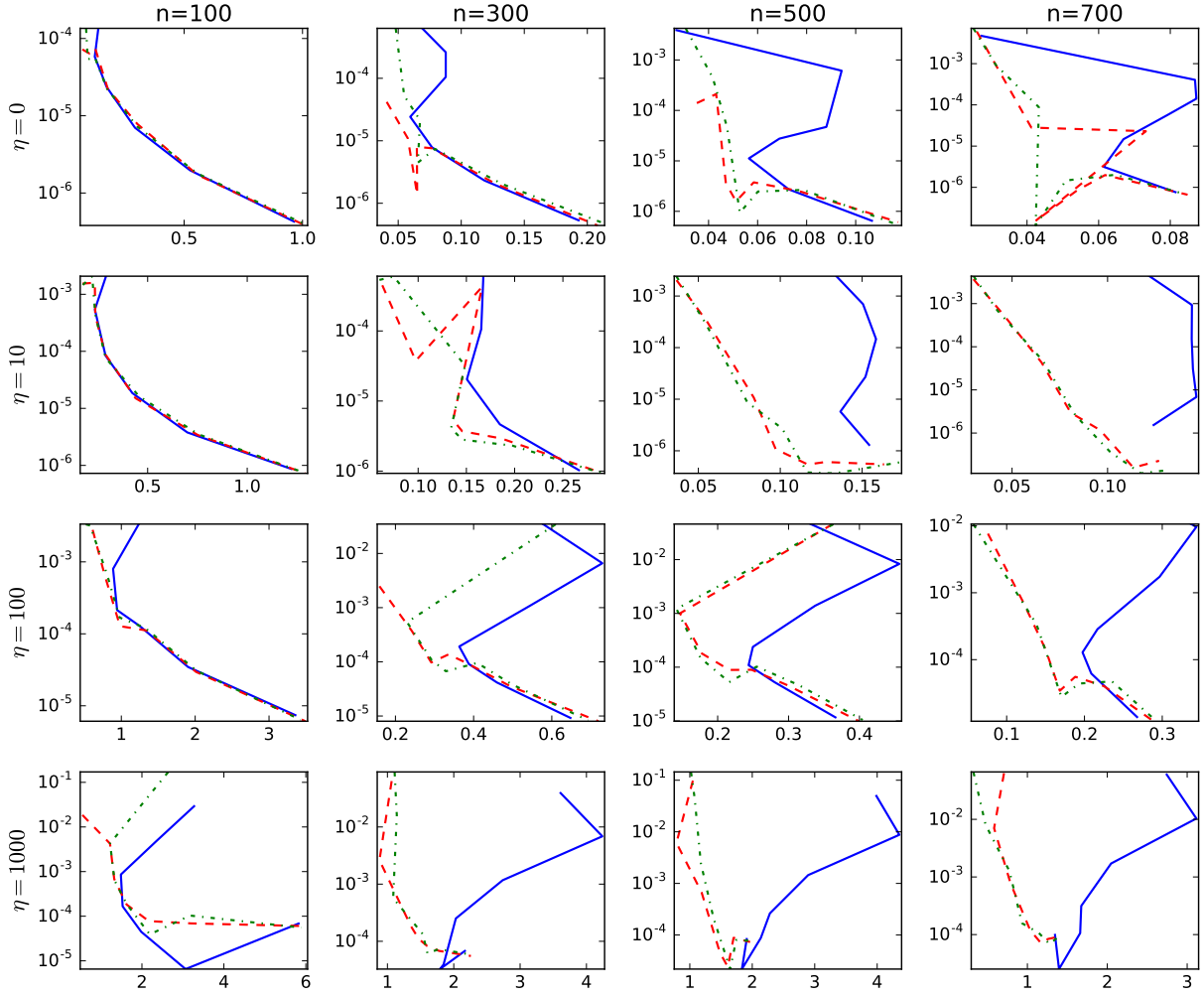


Figure 4: The number of normalized Krylov iterations employed by the Crank–Nicolson scheme (i.e. computational cost; on the x -axis) for the achieved accuracy at final time $t = 0.2$ (on the y -axis) is shown for equation (2) (linear diffusion-advection equation). The proposed step size controllers are shown as dashed red lines (penalized variant) and dash-dotted green lines (non-penalized variant), while the traditional step size controller is shown in solid blue. The grid size (n is the number of grid points) and the Péclet number η are varied.

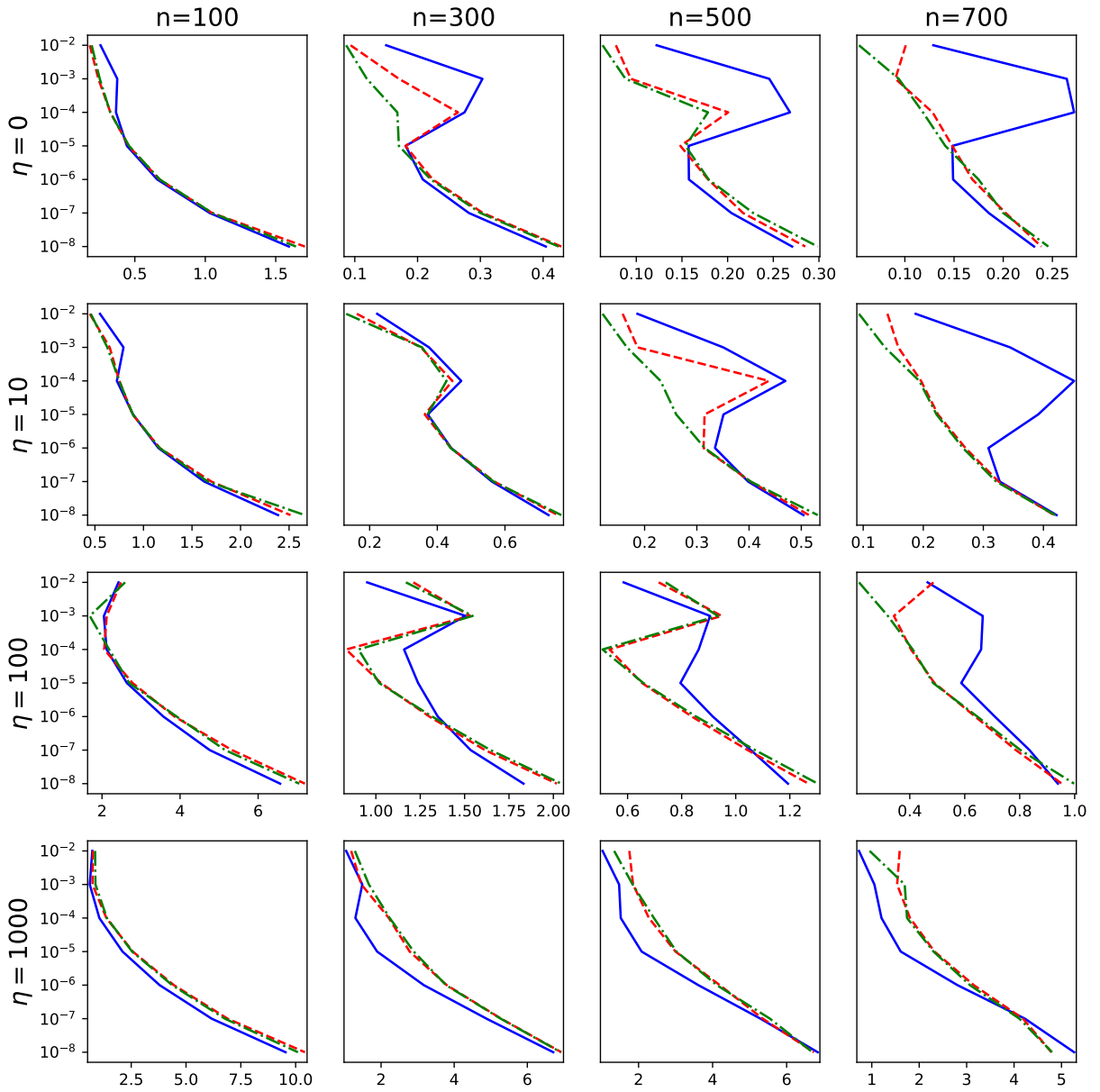


Figure 5: The number of normalized Krylov iterations employed by the SDIRK23 scheme (i.e. computational cost; on the x -axis) for a given tolerance (on the y -axis) is shown for equation (2) (linear diffusion-advection equation). The proposed step size controllers are shown as dashed red lines (penalized variant) and dash-dotted green lines (non-penalized variant), while the traditional step size controller is shown in solid blue. The grid size (n is the number of grid points) and the Péclet number η are varied.

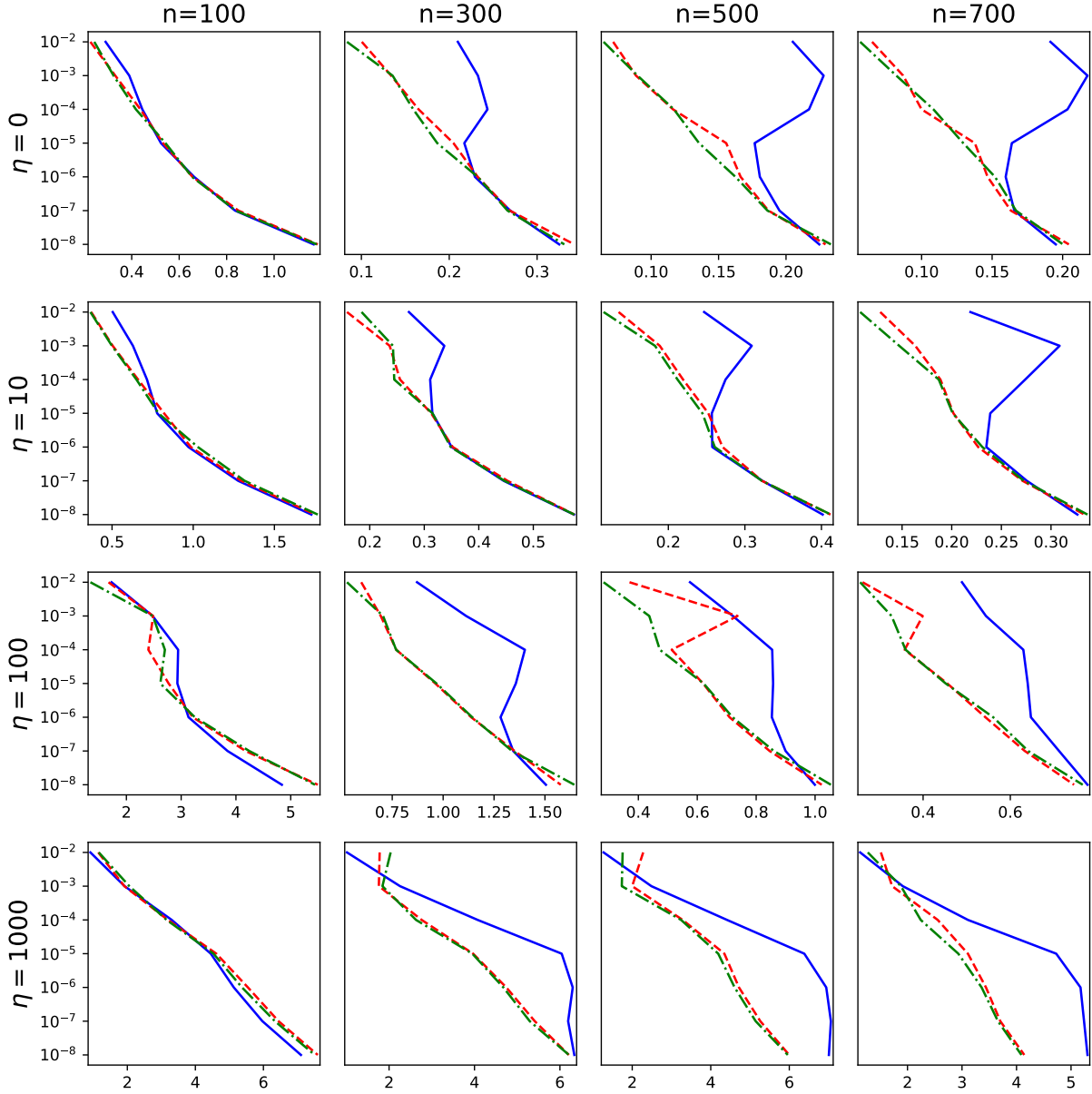


Figure 6: The number of normalized Krylov iterations employed by the SDIRK54 scheme (i.e. computational cost; on the x -axis) for a given tolerance (on the y -axis) is shown for equation (2) (linear diffusion-advection equation). The proposed step size controllers are shown as dashed red lines (penalized variant) and dash-dotted green lines (non-penalized variant), while the traditional step size controller is shown in solid blue. The grid size (n is the number of grid points) and the Péclet number η are varied.

being pulled towards 1 while other regions show a growth behavior. The Burgers' nonlinear, the strength of which is measured by η , steepens the gradients between these regions. The integration is performed until final time $t = 0.05$.

The work-precision diagrams for the Crank–Nicolson, SDIRK23, and SDIRK54 method are shown in Figures 7, 8, and 9, respectively. Overall, we see a significant improvement compared to the classic step size controller for all numerical methods and virtually all tolerances. The speedups observed range up to a factor of five and are most pronounced for medium to large tolerances.

In addition, in Figure 10 we show the achieved global error at a final time as a function of the number of Krylov iterations (this time for the SDIRK54 scheme). As expected, the advantage of the proposed approach compared to the traditional step size controller is even more pronounced according to this metric.

3.2. Porous medium equation

The second example is a porous media equation

$$\partial_t u(t, x) = \partial_{xx}(u(t, x)^m) + \eta \partial_x u(t, x), \quad (7)$$

where we have chosen $m = 2$. Periodic boundary conditions are imposed on $[0, 1]$ and the initial value is given by a rectangle

$$u(0, x) = 1 + H(x_1 - x) + H(x - x_2)$$

with $x_1 = 0.25$ and $x_2 = 0.6$. Note that in this problem we have a nonlinear diffusion, we could also write $\partial_{xx}(u^m) = \partial_x(mu^{m-1}\partial_x u)$, coupled to a linear advection. This results in a solution that is progressively more and more smooth even though we start from a discontinuous initial value. The equation is integrated until final time $t = 10^{-3}$.

The work-precision diagrams for the Crank–Nicolson, SDIRK23, and SDIRK54 method are shown in Figures 11, 12, and 13, respectively. For the Crank–Nicolson method and SDIRK23 we see a significant increase in performance, in particular, as we use more grid points to discretize the problem. The maximal achieved speedups for the numerical simulation shown is approximately a factor of four. The gains are significantly more modest for the SDIRK54 method. In this case maximal gains are on the order of 50% and they only manifest themselves at tolerances well below 10^{-6} . For low tolerances the proposed step size controller can be slightly slower than the traditional approach. It is in this regime that the penalized variant performs significantly better compared to the non-penalized variant (otherwise the two variants show similar performance). Nevertheless, overall a clear improvement in performance can still be observed.

3.3. Viscous Burgers' equation

The third example is the viscous Burgers' equation

$$\partial_t u(t, x) = \partial_{xx}u(t, x) - \eta u(t, x)\partial_x u(t, x). \quad (8)$$

Periodic boundary conditions are imposed on $[0, 1]$ and the initial value

$$u(0, x) = 1 + e \exp\left(\frac{-1}{1 - (2x - 1)^2}\right) + \frac{1}{2} \exp\left(-\frac{(x - x_0)^2}{2\sigma^2}\right),$$

where $x_0 = 0.9$ and $\sigma = 0.02$ is chosen. This corresponds to a \mathcal{C}^∞ bump at the tail of which a Gaussian of smaller amplitude is added. In this example the nonlinearity tries to create strong gradients, while the diffusion counteracts that. That is, η is a measure of how strong a resistance is provided to the homogenization of the solution. The problem is integrated to final time $t = 10^{-2}$.

The work-precision diagrams for the Crank–Nicolson, SDIRK23, and SDIRK54 method are shown in Figures 14, 15, and 16, respectively. For relatively low η only small improvements or even a slowdown can be observed. However, as we increase η the proposed step size controller shows a significant advantage for all numerical methods. Speedups up to a factor of two are observed, particular as the number of grid points is increased.

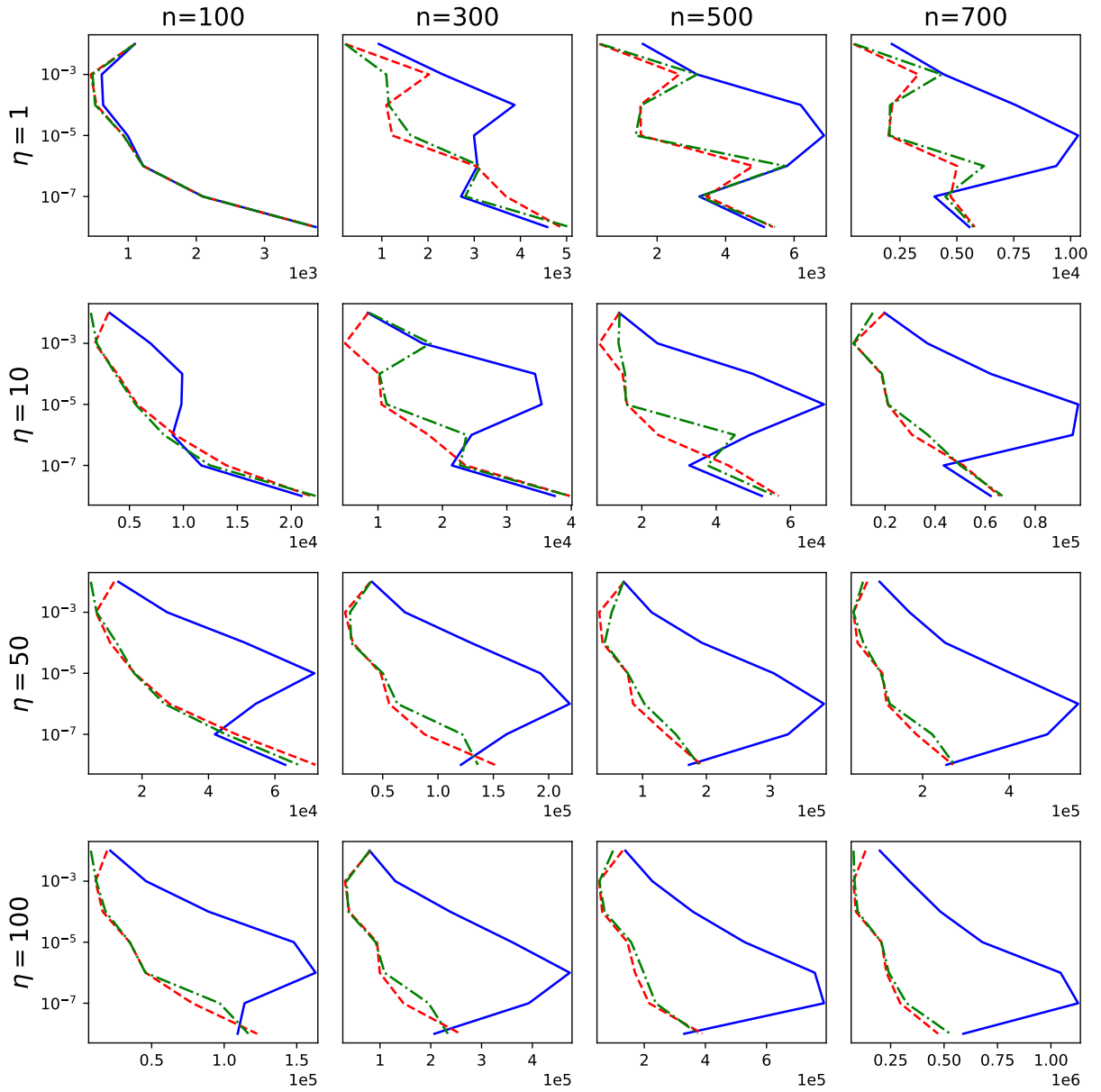


Figure 7: The number of Krylov iterations employed by the Crank–Nicolson scheme (i.e. computational cost; on the x -axis) for a given tolerance (on the y -axis) is shown for equation (6) (Burgers’ equation with a reaction term). The proposed step size controllers are shown as dashed red lines (penalized variant) and dash-dotted green lines (non-penalized variant), while the traditional step size controller is shown in solid blue. The grid size (n is the number of grid points) and the strength of the Burgers’ nonlinearity η are varied.

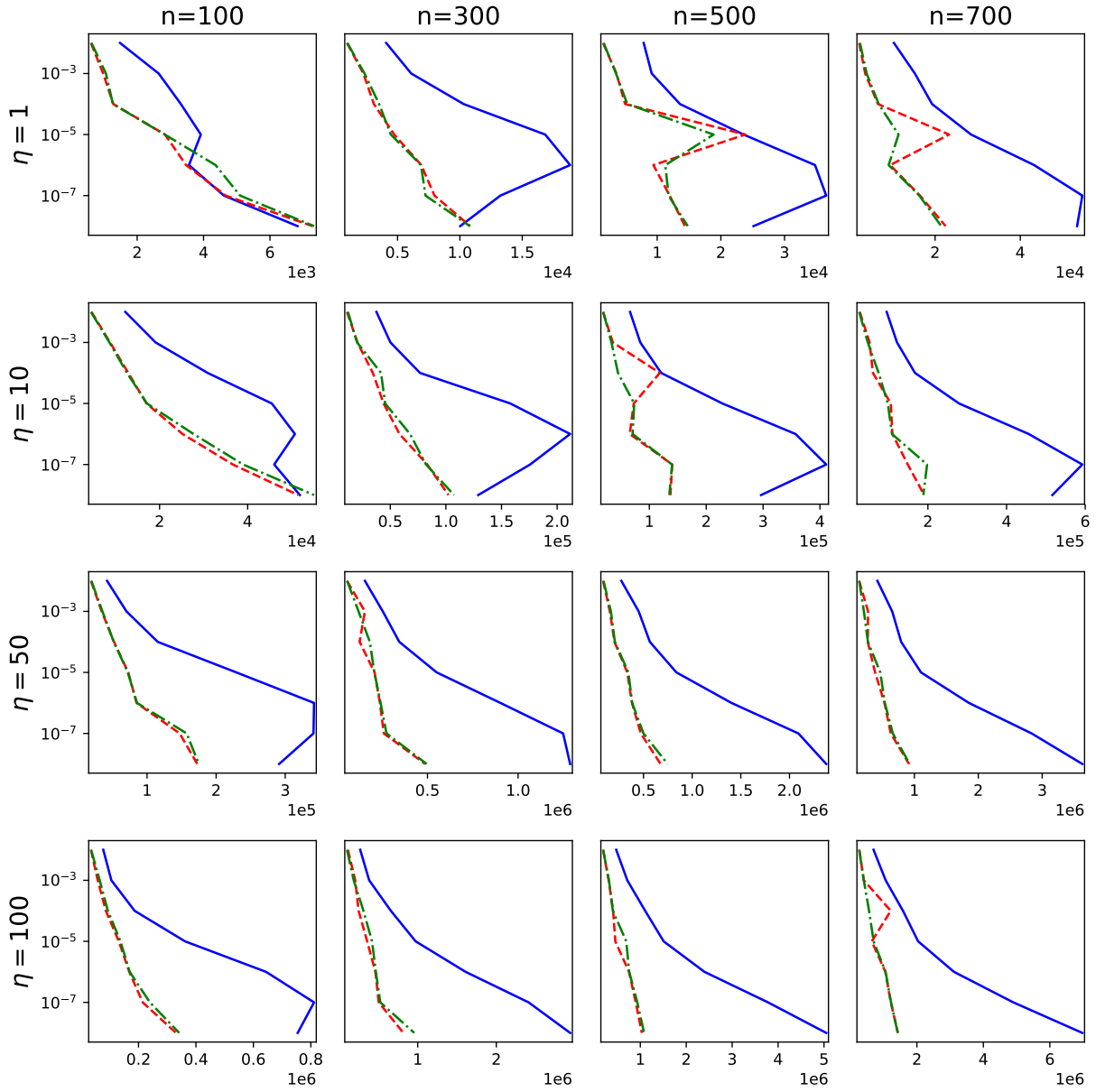


Figure 8: The number of Krylov iterations employed by the SDIRK23 scheme (i.e. computational cost; on the x -axis) for a given tolerance (on the y -axis) is shown for equation (6) (Burgers' equation with a reaction term). The proposed step size controllers are shown as dashed red lines (penalized variant) and dash-dotted green lines (non-penalized variant), while the traditional step size controller is shown in solid blue. The grid size (n is the number of grid points) and the strength of the Burgers' nonlinearity η are varied.

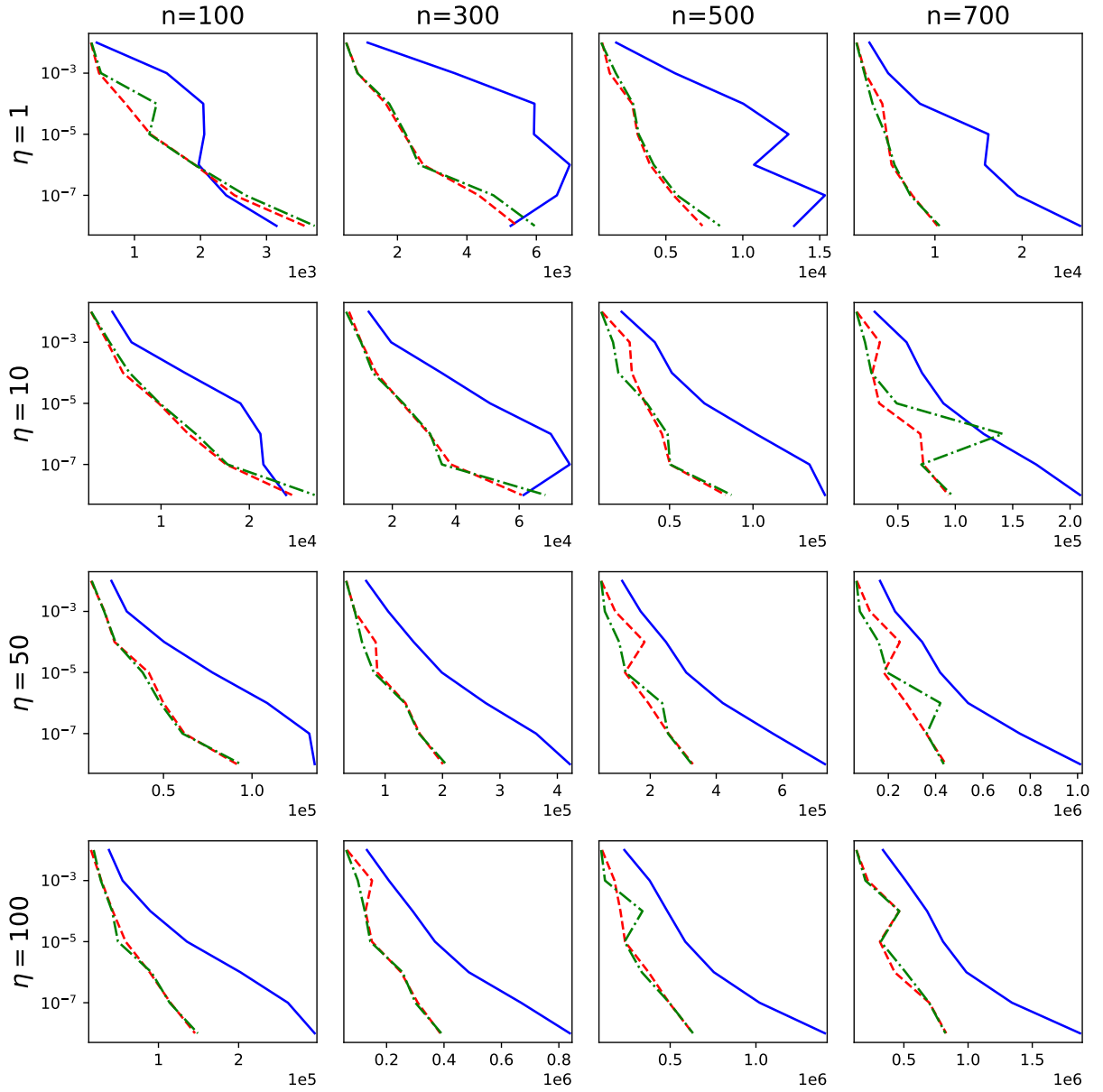


Figure 9: The number of Krylov iterations employed by the SDIRK54 scheme (i.e. computational cost; on the x -axis) for a given tolerance (on the y -axis) is shown for equation (6) (Burgers' equation with a reaction term). The proposed step size controllers are shown as dashed red lines (penalized variant) and dash-dotted green lines (non-penalized variant), while the traditional step size controller is shown in solid blue. The grid size (n is the number of grid points) and the strength of the Burgers' nonlinearity η are varied.

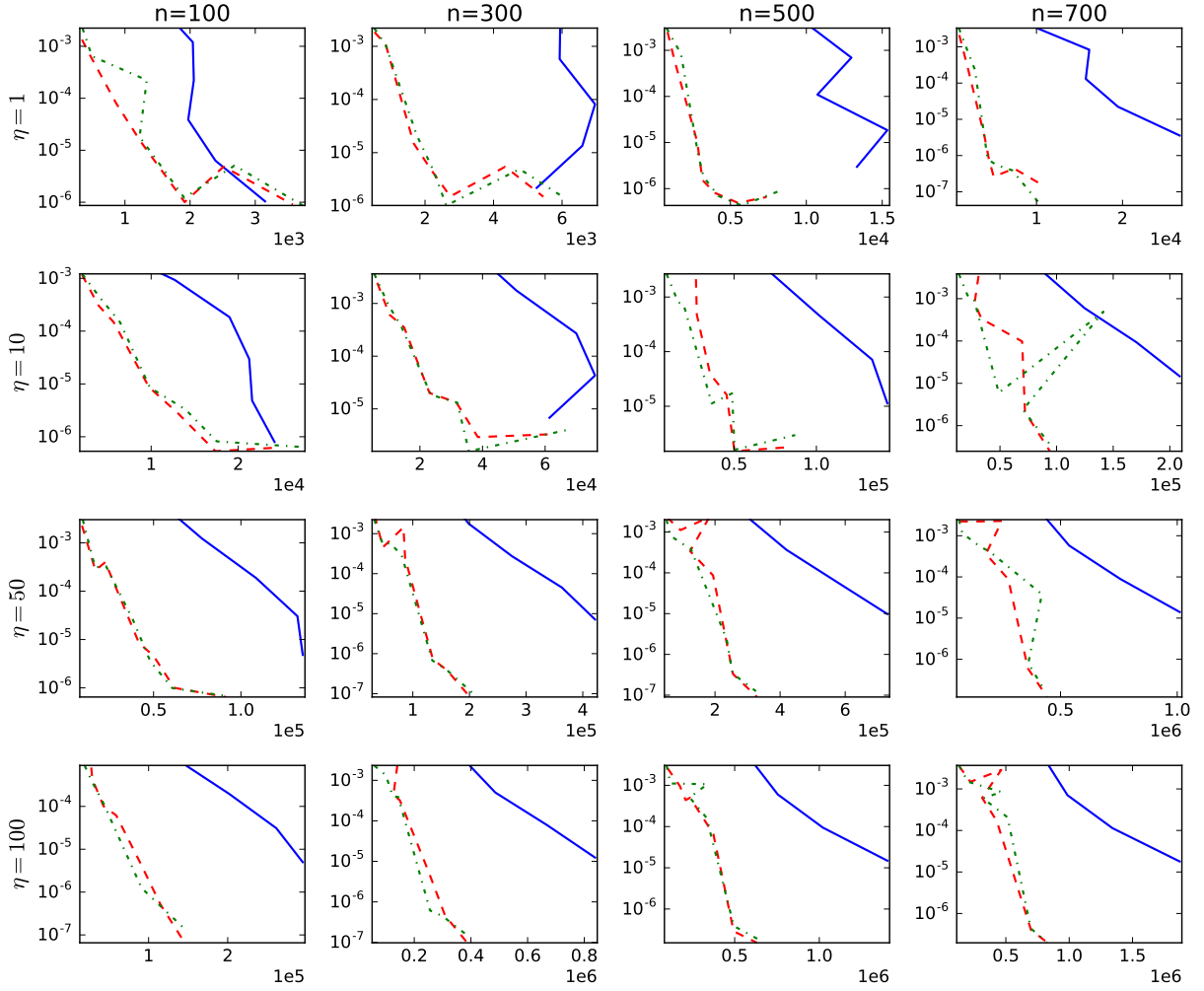


Figure 10: The number of Krylov iterations employed by the SDIRK54 scheme (i.e. computational cost; on the x -axis) for the achieved accuracy at final time $t = 0.05$ (on the y -axis) is shown for equation (6) (Burgers' equation with a reaction term). The proposed step size controllers are shown as dashed red lines (penalized variant) and dash-dotted green lines (non-penalized variant), while the traditional step size controller is shown in solid blue. The grid size (n is the number of grid points) and the strength of the Burgers' nonlinearity η are varied.

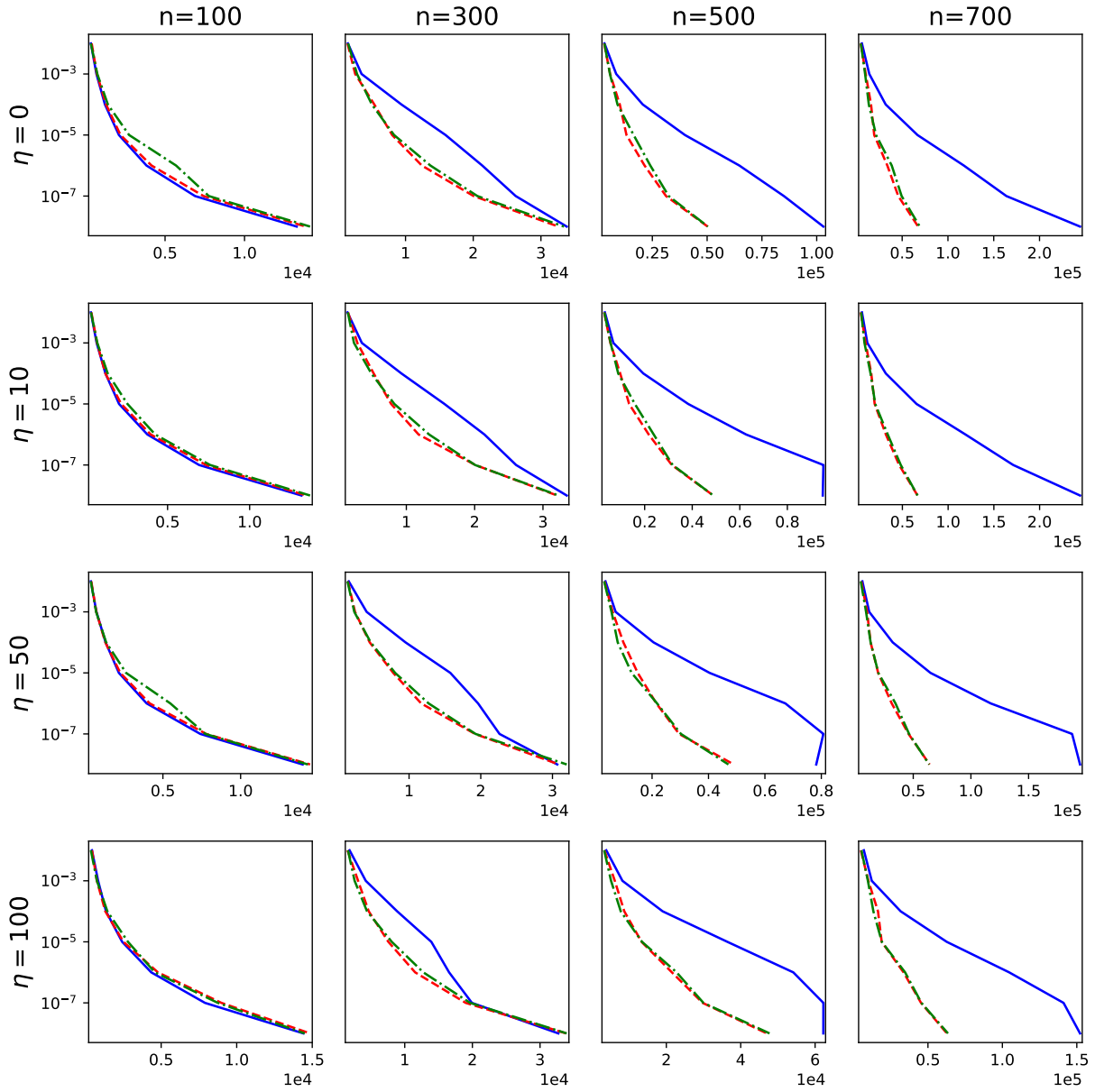


Figure 11: The number of Krylov iterations employed by the Crank–Nicolson scheme (i.e. computational cost; on the x -axis) for a given tolerance (on the y -axis) is shown for equation (7) (Porous medium equation). The proposed step size controllers are shown as dashed red lines (penalized variant) and dash-dotted green lines (non-penalized variant), while the traditional step size controller is shown in solid blue. The grid size (n is the number of grid points) and the speed of advection η are varied.

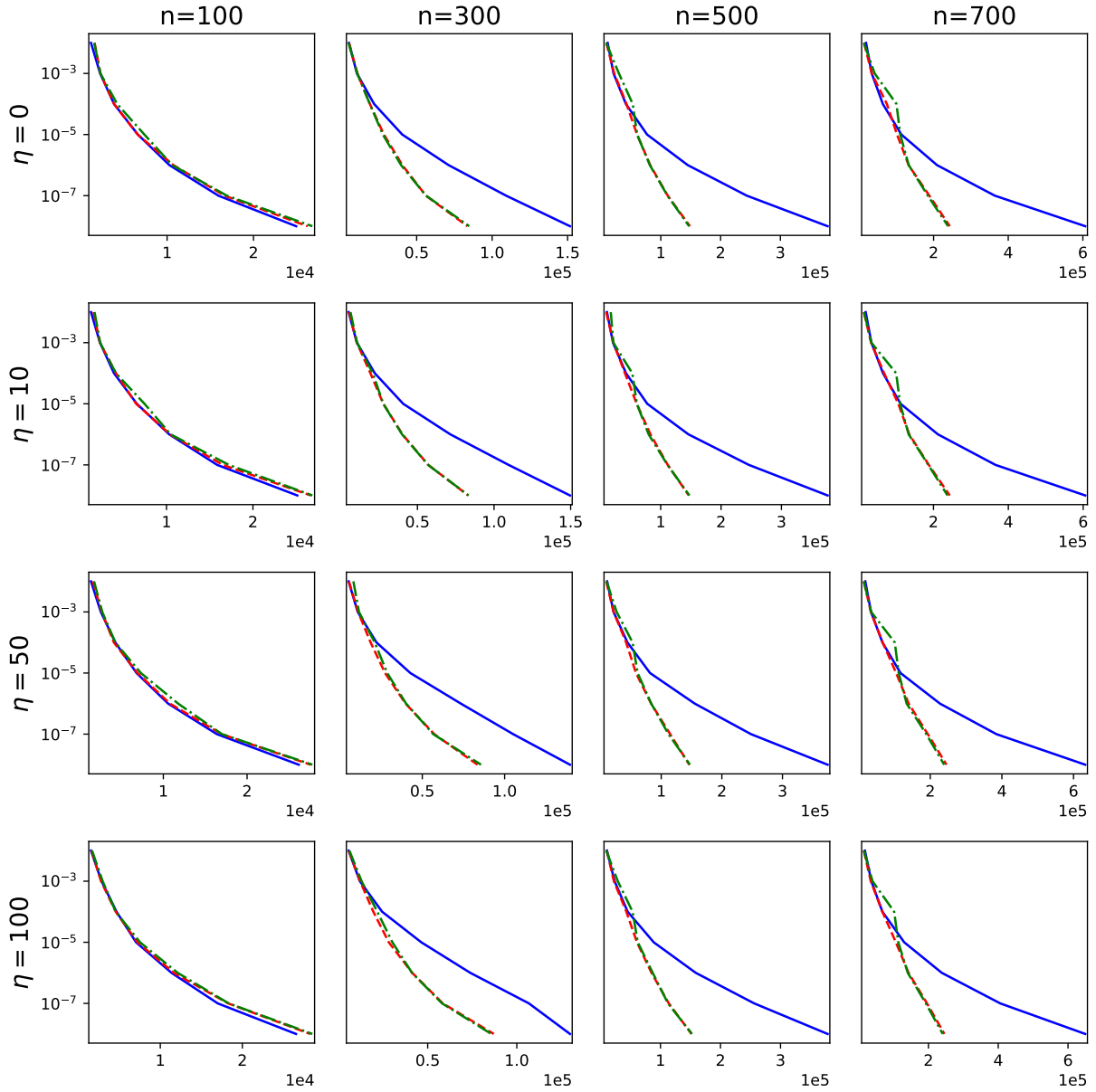


Figure 12: The number of Krylov iterations employed by the SDIRK23 scheme (i.e. computational cost; on the x -axis) for a given tolerance (on the y -axis) is shown for equation (7) (Porous medium equation). The proposed step size controllers are shown as dashed red lines (penalized variant) and dash-dotted green lines (non-penalized variant), while the traditional step size controller is shown in solid blue. The grid size (n is the number of grid points) and the speed of advection η are varied.

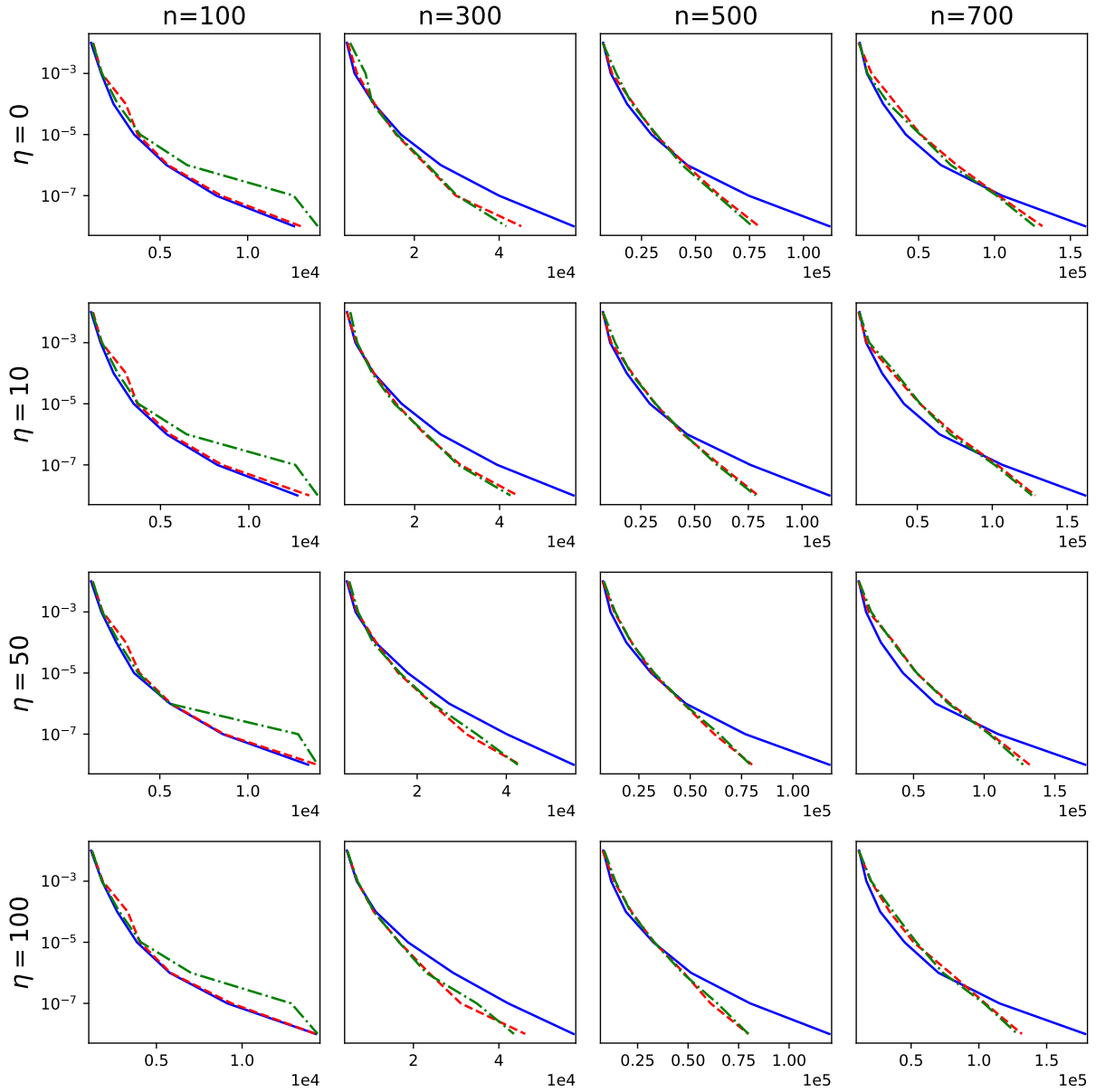


Figure 13: The number of Krylov iterations employed by the SDIRK54 scheme (i.e. computational cost; on the x -axis) for a given tolerance (on the y -axis) is shown for equation (7) (Porous medium equation). The proposed step size controllers are shown as dashed red lines (penalized variant) and dash-dotted green lines (non-penalized variant), while the traditional step size controller is shown in solid blue. The grid size (n is the number of grid points) and the speed of advection η are varied.

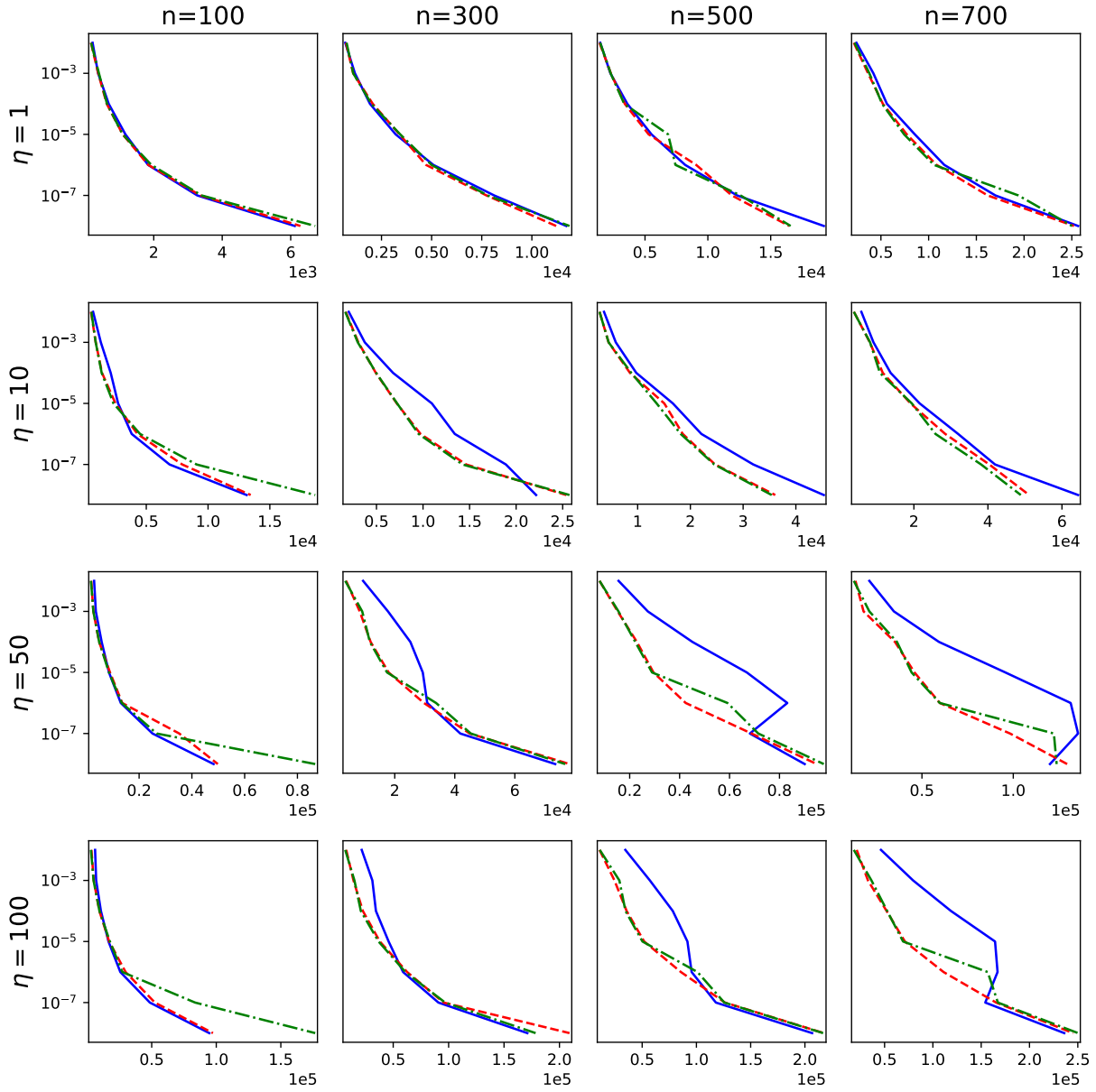


Figure 14: The number of Krylov iterations employed by the Crank–Nicolson scheme (i.e. computational cost; on the x -axis) for a given tolerance (on the y -axis) is shown for equation (8) (viscous Burgers’ equation). The proposed step size controllers are shown as dashed red lines (penalized variant) and dash-dotted green lines (non-penalized variant), while the traditional step size controller is shown in solid blue. The grid size (n is the number of grid points) and the strength of the nonlinear advection η are varied.

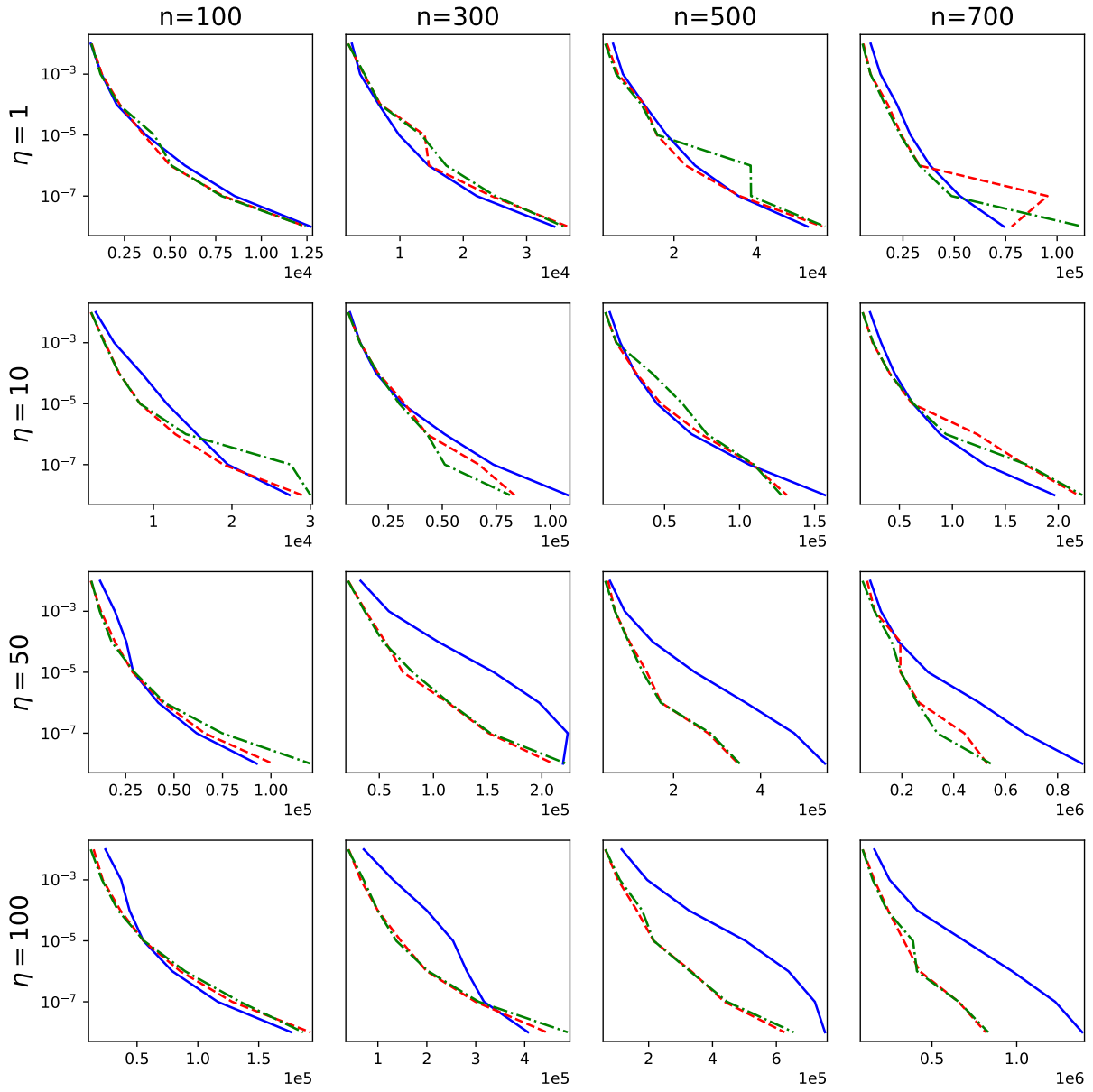


Figure 15: The number of Krylov iterations employed by the SDIRK23 scheme (i.e. computational cost; on the x -axis) for a given tolerance (on the y -axis) is shown for equation (8) (viscous Burgers' equation). The proposed step size controllers are shown as dashed red lines (penalized variant) and dash-dotted green lines (non-penalized variant), while the traditional step size controller is shown in solid blue. The grid size (n is the number of grid points) and the strength of the nonlinear advection η are varied.

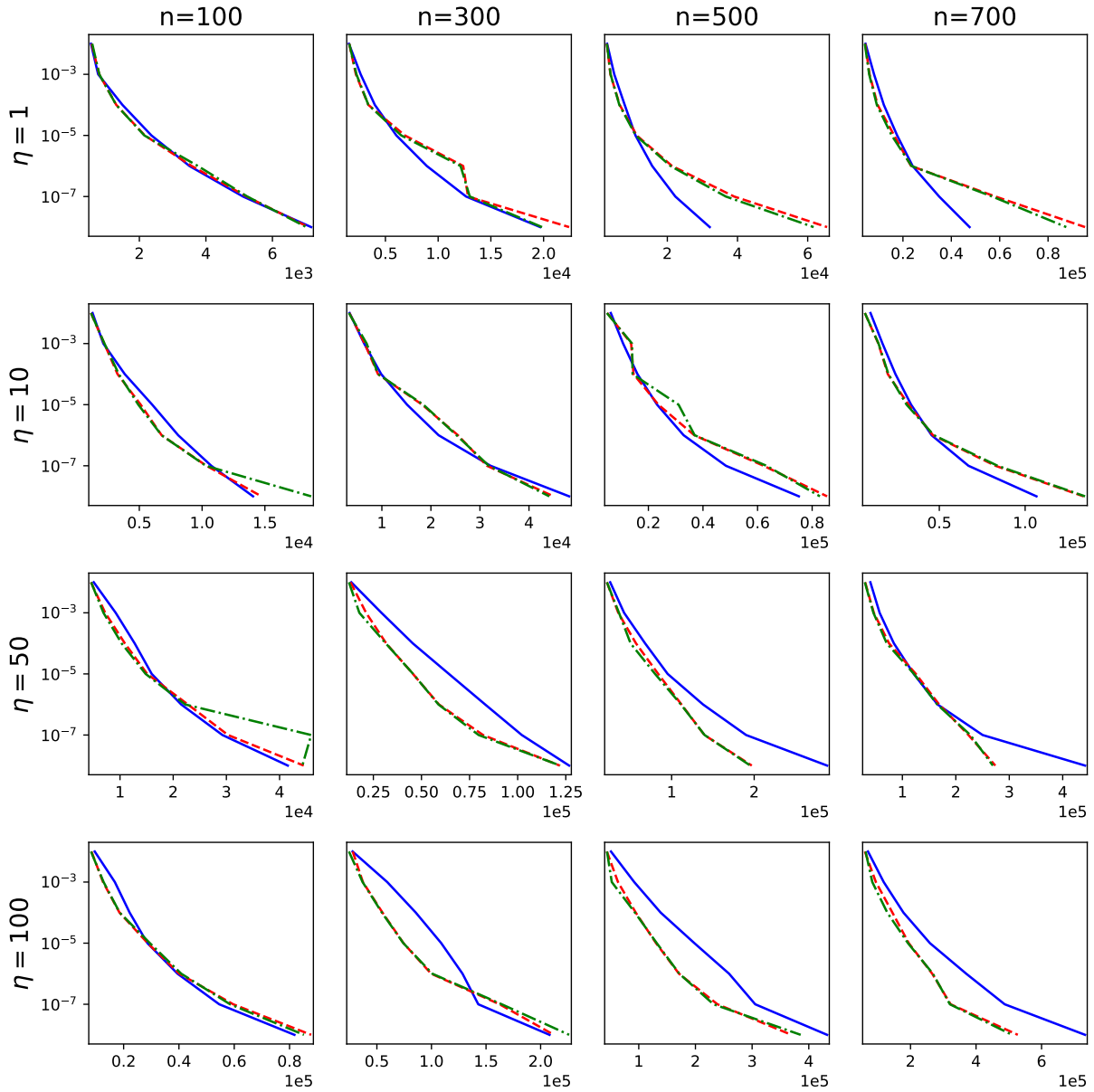


Figure 16: The number of Krylov iterations employed by the SDIRK54 scheme (i.e. computational cost; on the x -axis) for a given tolerance (on the y -axis) is shown for equation (8) (viscous Burgers' equation). The proposed step size controllers are shown as dashed red lines (penalized variant) and dash-dotted green lines (non-penalized variant), while the traditional step size controller is shown in solid blue. The grid size (n is the number of grid points) and the strength of the nonlinear advection η are varied.

3.4. Allen–Cahn equation

As the fourth example we consider the one-dimensional Allen–Cahn equation

$$\partial_t u(t, x) = \partial_{xx} u(t, x) + \eta u(t, x)(1 - u(t, x)^2). \quad (9)$$

Periodic boundary conditions are imposed on $[0, 1]$ and the following initial value

$$u(0, x) = A(1 + \cos \omega_1 x),$$

with $A = \frac{1}{10}$ and $\omega_1 = 2\pi$ is used. This problem does not include an advection term. As a consequence, the linear part of the right-hand side is a symmetric matrix. The interesting behavior of the Allen–Cahn equation is due to the fact that the nonlinear reaction term pulls the solution to either 0, 1, or -1 , while the diffusion tries to homogenize the solution. This results, for larger η , in regions of space that are separated by relatively sharp gradients. The problem is integrated to final time $t = 2 \cdot 10^{-2}$.

The work-precision diagrams for the Crank–Nicolson, SDIRK23, and SDIRK54 method are shown in Figures 17, 18, and 19, respectively. For the Crank–Nicolson and the SDIRK23 scheme large increases in performance can be observed for large η . For the SDIRK54 method the proposed step size controller shows significant savings in computational effort for $\eta \leq 100$ and similar performance for $\eta = 1000$. Although there are some small differences between the penalized and non-penalized variants, in the present test these two methods perform very similar.

4. Brusselator in two dimensions

As the final example we consider the two-dimensional Brusselator given by

$$\begin{aligned} \partial_t u(t, x, y) &= \alpha \Delta u(t, x, y) + 1 + u^2 v - 4.4u + f(t, x, y) \\ \partial_t v(t, x, y) &= \alpha \Delta v(t, x, y) + 3.4u - u^2 v, \end{aligned} \quad (10)$$

where $\Delta = \partial_{xx} + \partial_{yy}$ is the Laplacian and $\alpha = 0.1$. Periodic boundary conditions on $[0, 1]^2$ are imposed and the following initial value

$$u(0, x, y) = 22y(1 - y)^{3/2}, \quad v(0, x, y) = 27x(1 - x)^{3/2}$$

is selected. The function f is a source term and is chosen such that $f(t, x, y) = 5$ if $(x - 0.3)^2 + (y - 0.6)^2 \leq 0.1^2$ and $t \geq 1.1$. Otherwise $f(t, x, y)$ is set to zero. The problem is integrated to final time $t = 11.5$. This is the problem considered in [11, p. 151–152].

The work-precision diagrams for the Crank–Nicolson, SDIRK23, and SDIRK54 methods are shown in Figure 20. The penalized variant of the proposed step size controller shows superior performance in virtually all configuration. The non-penalized variants performs worse. This is particularly true for the finest grid with the SDIRK23 and SDIRK54 schemes, where it does not converge in a reasonable amount of time. However, in the other configurations it is still able to significantly outperform the traditional step size controller in the low to medium precision regime. The penalized version of the proposed step size controller mostly avoids the inverse C curve and is more robust. The latter is most apparent for the SDIRK23 scheme, where the standard step size controller, for tolerances above 10^{-6} , does not produce a solution within a reasonable amount of time (note that this issue was also reported in the context of CVODE applied to a magnetohydrodynamics problem [7]).

5. Conclusion

We have demonstrated that the proposed adaptive step size selection strategy result in significant improvements compared to more traditional approaches in the context of a number of one-dimensional test problems. Speedups of up to a factor of five have been observed and significant increases in performance

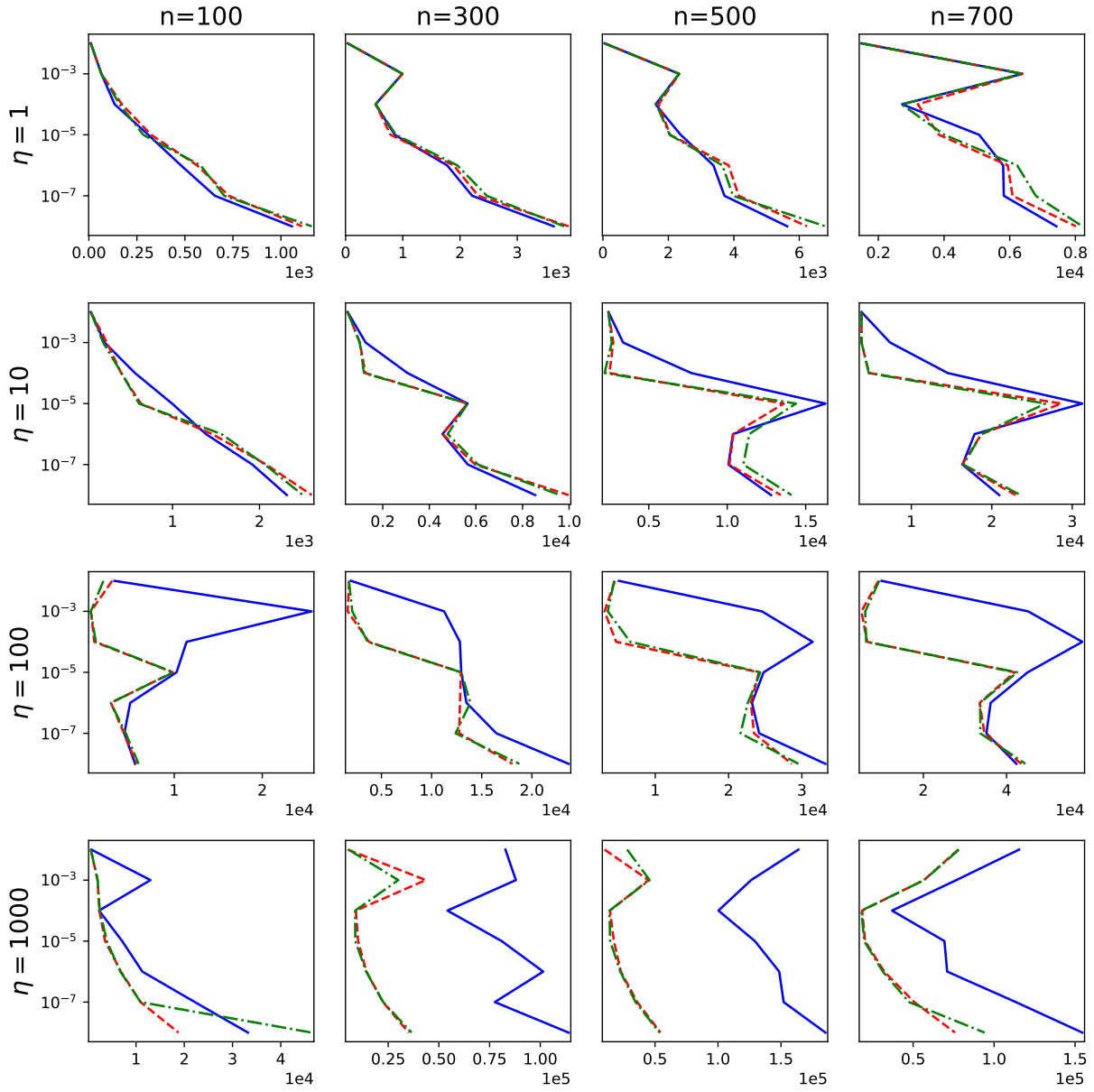


Figure 17: The number of Krylov iterations employed by the Crank–Nicolson scheme (i.e. computational cost; on the x -axis) for a given tolerance (on the y -axis) is shown for equation (9) (Allen–Cahn equation). The proposed step size controllers are shown as dashed red lines (penalized variant) and dash-dotted green lines (non-penalized variant), while the traditional step size controller is shown in solid blue. The grid size (n is the number of grid points) and the strength of the nonlinear reaction η are varied.

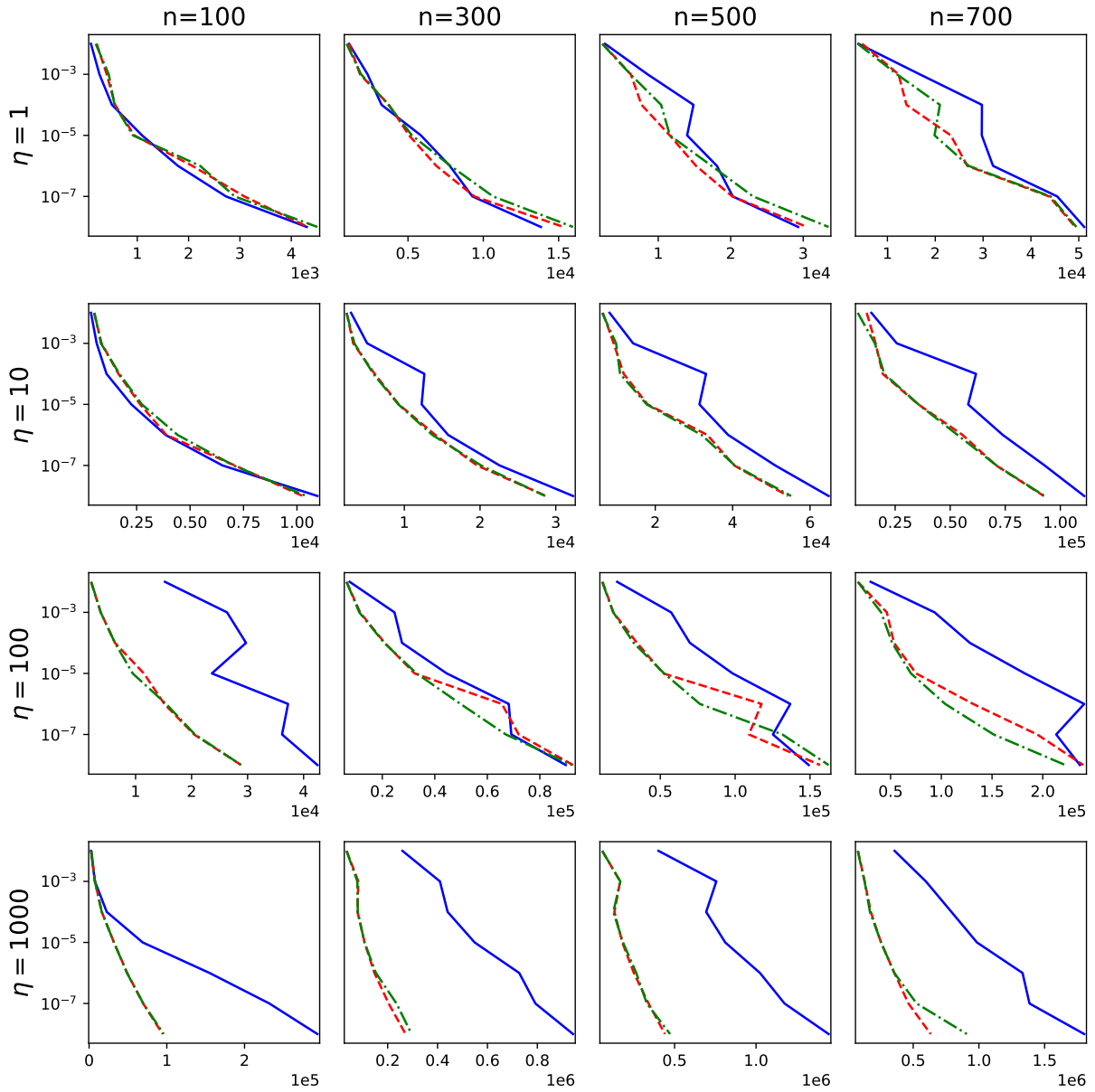


Figure 18: The number of Krylov iterations employed by the SDIRK23 scheme (i.e. computational cost; on the x -axis) for a given tolerance (on the y -axis) is shown for equation (9) (Allen-Cahn equation). The proposed step size controllers are shown as dashed red lines (penalized variant) and dash-dotted green lines (non-penalized variant), while the traditional step size controller is shown in solid blue. The grid size (n is the number of grid points) and the strength of the nonlinear reaction η are varied.

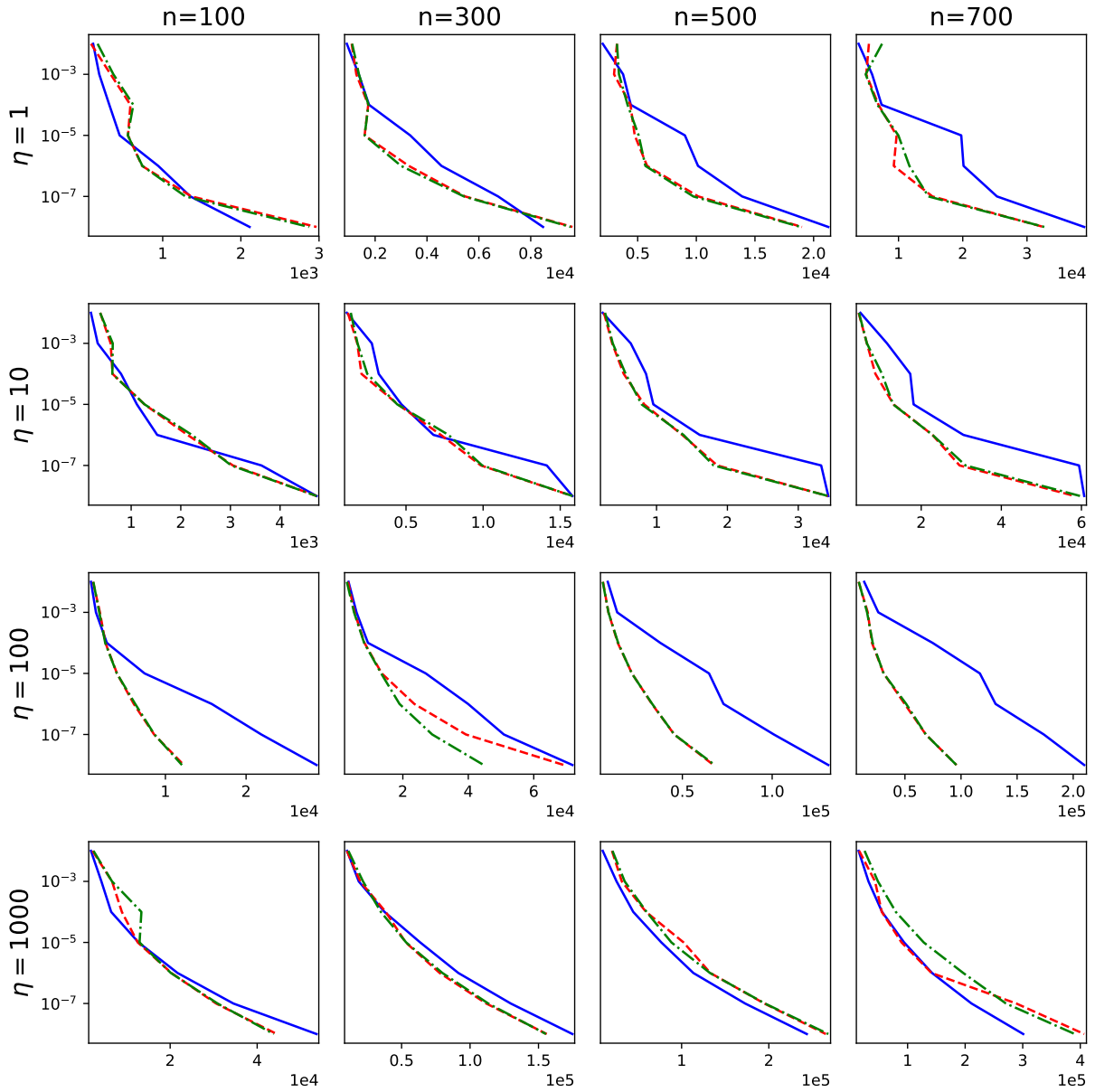


Figure 19: The number of Krylov iterations employed by the SDIRK54 scheme (i.e. computational cost; on the x -axis) for a given tolerance (on the y -axis) is shown for equation (9) (Allen-Cahn equation). The proposed step size controllers are shown as dashed red lines (penalized variant) and dash-dotted green lines (non-penalized variant), while the traditional step size controller is shown in solid blue. The grid size (n is the number of grid points) and the strength of the nonlinear reaction η are varied.

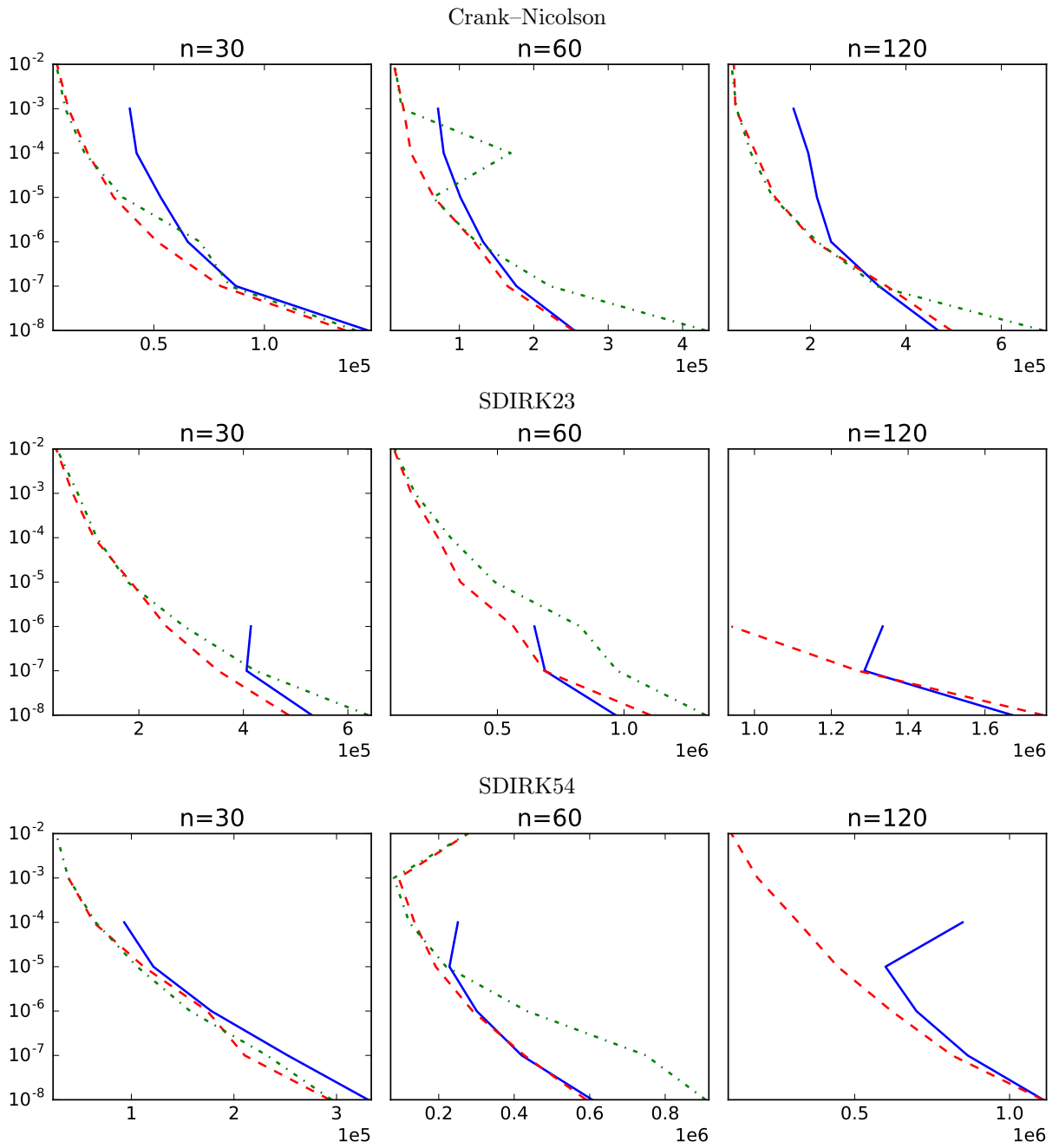


Figure 20: The number of Krylov iterations employed by the Crank–Nicolson/SDIRK23/SDIRK54 schemes (i.e. computational cost; on the x -axis) for a given tolerance (on the y -axis) is shown for equation (10) (the two-dimensional Brusselator). The proposed step size controllers are shown as dashed red lines (penalized variant) and dash-dotted green lines (non-penalized variant), while the traditional step size controller is shown in solid blue. The grid size (n is the number of grid points per direction) is varied.

are seen in almost all problems. In addition, the inverse C curve is straightened out in almost all configurations which makes the step size controller more predictable in practice. In addition, we have considered the two-dimensional Brusselator, where similar conclusions can be drawn for the penalized variant.

It is also interesting to note that the speedup observed is most pronounced for the Crank–Nicolson method, which is still widely used by physicists and engineers. This might be considered a further disadvantage of this method (i.e. traditional step size controllers do not work as well). Whether this is generally true for methods that fail to be L-stable might warrant further investigation.

The method proposed here is relatively simple since it only requires a limited set of parameters. Consequently, optimizing for these parameters is relatively straightforward and our approach, which only uses selected samples of a linear problem, demonstrates that such an approach can be successfully generalized to different linear and even nonlinear problems. However, one could envisage an approach that makes use of data obtained in previous time steps as well as allows for more general mappings. To train such a model, however, would require an extensive set of representative test problems. We consider this as future work. In addition, our plan is to extend the step size controller proposed here to more elaborate implicit methods (such as Radau and Gauss methods) and consider physically more realistic problems in multiple dimensions.

References

- [1] U. M. Ascher, S. J. Ruuth, and R. J. Spiteri. Implicit-explicit Runge-Kutta methods for time-dependent partial differential equations. *Applied Numerical Mathematics*, 25(2-3):151–167, 1997.
- [2] D. S. Blom, P. Birken, H. Bijl, F. Kessels, A. Meister, and A. H. van Zuijlen. A comparison of Rosenbrock and ESDIRK methods combined with iterative solvers for unsteady compressible flows. *Advances in Computational Mathematics*, 42(6):1401–1426, 2016.
- [3] M. Caliari, P. Kandolf, A. Ostermann, and S. Rainer. The Leja method revisited: Backward error analysis for the matrix exponential. *SIAM Journal on Scientific Computing*, 38(3):A1639–A1661, 2016.
- [4] J. R. Cash. Diagonally implicit Runge-Kutta formulae with error estimates. *IMA Journal of Numerical Analysis*, 24(3):293–301, 1979.
- [5] J. R. Dormand and P. J. Prince. A family of embedded Runge-Kutta formulae. *Journal of Computational and Applied Mathematics*, 6(1):19–26, 1980.
- [6] S. Eckert, H. Baaser, D. Gross, and O. Scherf. A BDF2 integration method with step size control for elasto-plasticity. *Computational Mechanics*, 34(5):377–386, 2004.
- [7] L. Einkemmer, M. Tokman, and J. Loffeld. On the performance of exponential integrators for problems in magnetohydrodynamics. *Journal of Computational Physics*, 330:550–565, 2017.
- [8] K. Gustafsson. Control-theoretic techniques for stepsize selection in implicit Runge-Kutta methods. *ACM Transactions on Mathematical Software*, 20(4):496–517, 1994.
- [9] K. Gustafsson, M. Lundh, and G. Söderlind. A PI stepsize control for the numerical solution of ordinary differential equations. *BIT Numerical Mathematics*, 28(2):270–287, 1988.
- [10] K. Gustafsson and G. Söderlind. Control strategies for the iterative solution of nonlinear equations in ODE solvers. *SIAM Journal on Scientific Computing*, 18(1):23–40, 1997.
- [11] E. Hairer and G. Wanner. *Solving Ordinary Differential Equations II, Stiff and Differential-Algebraic Problems*. Springer Berlin Heidelberg, 1996.
- [12] E. Hairer, G. Wanner, and S. P. Nørsett. *Solving Ordinary Differential Equations I, Nonstiff Problems*, volume 8. Springer Berlin Heidelberg, 1993.

- [13] G. Hall. A new stepsize strategy for explicit Runge-Kutta codes. *Advances in Computational Mathematics*, 3(4):343–352, 1995.
- [14] A. C. Hindmarsh and R. Serban. User Documentation for ccode v2.9.0. https://computation.llnl.gov/sites/default/files/public/cv_guide.pdf, 2016.
- [15] M. Hochbruck, C. Lubich, and H. Selhofer. Exponential integrators for large systems of differential equations. *SIAM Journal on Scientific Computing*, 19(5):1552–1574, 1998.
- [16] J. Loffeld and M. Tokman. Comparative performance of exponential, implicit, and explicit integrators for stiff systems of ODEs. *Journal of Computational and Applied Mathematics*, 241:45–67, 2013.
- [17] V. T. Luan, M. Tokman, and G. Rainwater. Preconditioned implicit-exponential integrators (IMEXP) for stiff PDEs. *Journal of Computational Physics*, 335:846–864, 2017.
- [18] M. Narayanamurthi, P. Tranquilli, A. Sandu, and M. Tokman. EPIRK-W and EPIRK-K time discretization methods. *arXiv preprint, arXiv:1701.06528*, 2017.
- [19] L. F. Shampine. Error estimation and control for ODEs. *Journal of Scientific Computing*, 25(1):3–16, 2005.
- [20] L. F. Shampine and L. S. Baca. Error estimators for stiff differential equations. *Journal of Computational and Applied Mathematics*, 11(2):197–207, 1984.
- [21] G. Söderlind. Automatic control and adaptive time-stepping. *Numerical Algorithms*, 31(1-4):281–310, 2002.
- [22] G. Söderlind. Time-step selection algorithms: Adaptivity, control, and signal processing. *Applied Numerical Mathematics*, 56(3-4):488–502, 2006.
- [23] A. Usman and G. Hall. Alternative stepsize strategies for Adams predictor–corrector codes. *Journal of Computational and Applied Mathematics*, 116(1):105–120, 2000.
- [24] R. Weiner and B.A. Schmitt. Order results for Krylov-W-methods. *Computing*, 61(1):69–89, 1998.